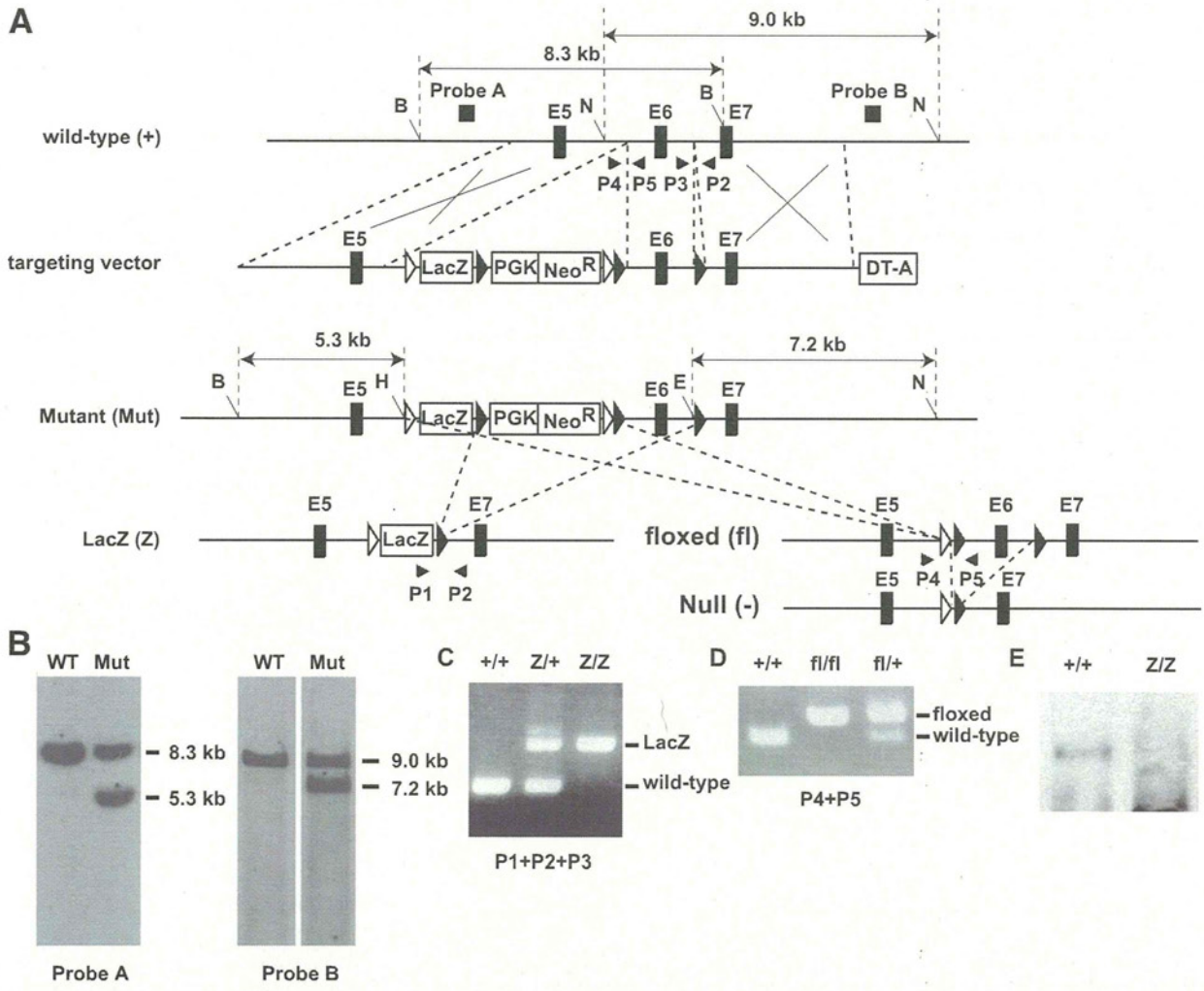

FIG. 1. Strategic scheme for targeted disruption of mouse *Phf2*. *A*: Targeting strategy with positive/negative selection. Strategy of genomic Southern blotting in the screening for homologous recombinant embryonic stem cell clones is also included. E5, E6, and E7 represent exon 5, exon 6, and exon 7 of *Phf2*, respectively. B, H, E, and N represent BglII, HindIII, EcoRI, and NsiI cut sites, respectively. P1, P2, P3, P4, and P5 represent locations of primers used in *C* and *D*. ▷, the *LoxP* sites; ▶, *Frt* sites. *B*: Southern blotting analysis of targeted embryonic stem cell clones. Restriction enzymes used for screening recombination events with probe A were BglII and HindIII. An 8.3-kb fragment in WT and a 5.3-kb fragment after homologous recombination were expected with probe A. Restriction enzymes used for screening recombination events with probe B were EcoRI and NsiI. A 9.0-kb fragment in WT and a 7.2-kb fragment after homologous recombination were expected with probe B. *C*: To detect the presence of the *LacZ* allele (Z) and the WT allele (+),primers P1, P2, and P3 were used. The PCR bands of the WT allele (242 bp) and the *LacZ* allele (495 bp) are indicated. *D*: To detect the presence of the floxed allele (*fl*) and the WT allele (+),primers P4 and P5 were used. The PCR bands of the WT allele (162 bp) and the floxed allele (245 bp) are indicated. *E*: Western blot analysis of PHF2 protein expression in *Phf2*$^{Z/Z}$ mice. Extracts of mouse embryonic fibroblasts from WT or *Phf2*$^{Z/Z}$ were immunoprecipitated and detected with anti-PHF2 antibody. WT, wild type.

observed in subcutaneous WAT to an extent similar to that in epididymal WAT (P = 0.06) but to a lesser extent in mesenteric WAT (Fig. 3*B*). Additionally, female *Phf2*$^{Z/Z}$ mice exhibited a similar reduced weight of gonadal WAT as observed in male mice (Fig. 3*C*). However, these weight reductions in adipose tissues seemed to be limited to a young age because there was no significant difference of WAT weights between *Phf2*$^{Z/Z}$ and wild-type littermates when the mice reached 8 weeks of age (Supplementary Fig. 1). To elucidate whether the decreased weight of WAT was caused by a reduction of lipid droplets per cell or adipocyte number, we measured adipocyte size and number in epididymal WAT of *Phf2*$^{Z/Z}$ and wild-type littermates. Evaluation of the mean adipocyte area in the section of WAT revealed that *Phf2*$^{Z/Z}$ mice have smaller adipocytes than do control littermates (Fig. 3*D*). Furthermore, counting the number of adipocytes in WAT revealed that *Phf2*$^{Z/Z}$ mice have fewer adipocytes in adipose tissue (Fig. 3*E*). These data suggest that the decreased weight of WAT in *Phf2*$^{Z/Z}$ mice was caused by a reduction in both the size and the number of adipocytes. Because impaired adipogenesis often results in decreased size (20) and a decreased number of adipocytes, we used microarray analysis to compare the gene expression profiles in WAT between *Phf2*$^{Z/Z}$ mice and control littermates. As a result, the expression of various genes associated with adipogenesis, such as *Pparg*, *Cebpa*, *Fabp4*, *Adipoq*, *LPL*, *Plin2*, and *Cd36*, tended to be decreased in *Phf2*$^{Z/Z}$ mice (Supplementary Fig. 2). The expression levels of more than half of these genes were significantly reduced when confirmed by real-time quantitative PCR (qPCR) (Fig. 3*F*). These data suggest that decreased WAT weight in *Phf2*$^{Z/Z}$ mice resulted, at least in part, from impaired adipogenesis in these mice. Finally, we measured insulin sensitivity in

A

At Birth

+/+	Z/+	Z/Z	Total
9	14	11	34
26%	41%	32%	100%

B

At 2 weeks

+/+	Z/+	Z/Z	Total
52	91	17**	160
33%	57%	11%	100%

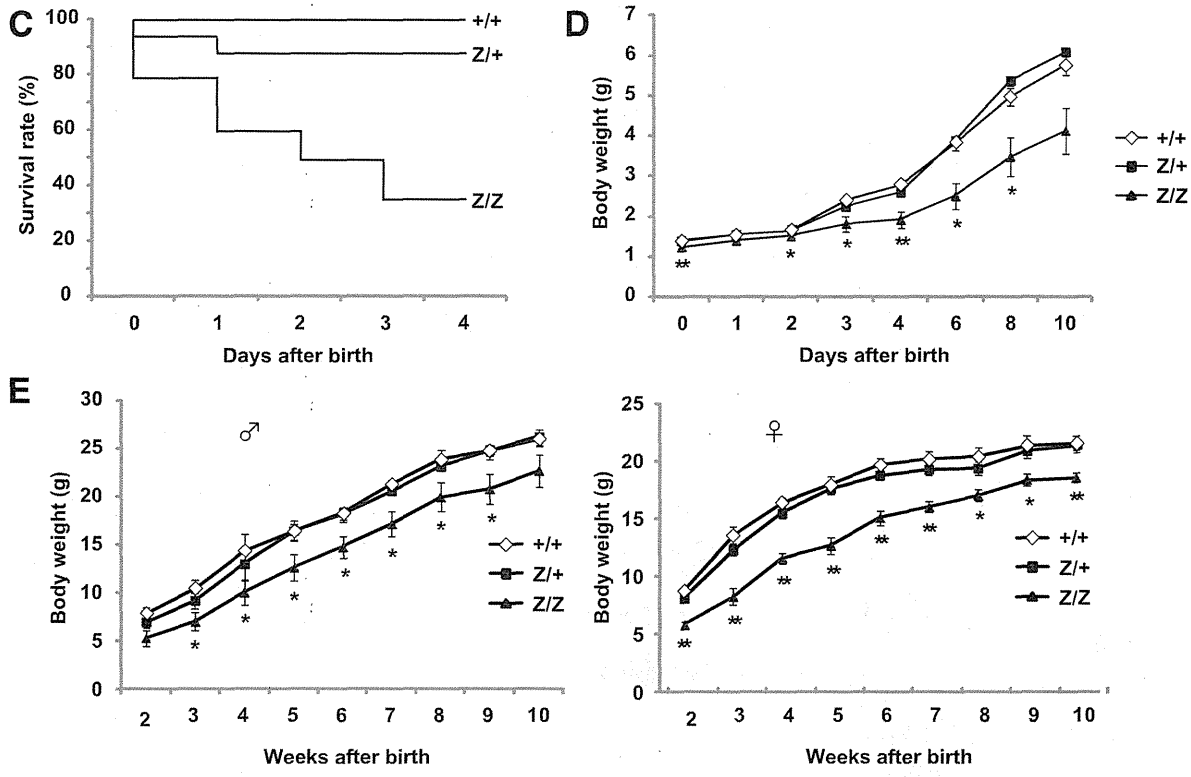

FIG. 2. Physiological features of systemic *Phf2* knockout mice. *A*: Genotypes of progeny of crosses between $Phf2^{Z/+}$ at birth. *B*: Genotypes of progeny of crosses between $Phf2^{Z/+}$ at 2 weeks of age. *C*: Survival rate of progeny of crosses between $Phf2^{Z/+}$. *D*: Growth curves of wild-type, heterozygous, and homozygous *Phf2* knockout mice until 10 days after birth. *E*: Growth curves of male mice and female mice of indicated genotypes between 2 and 10 weeks of age. ◇, wild-type mice (+/+); ■, heterozygous *Phf2* knockout mice (*Z*/+); ▲, homozygous *Phf2* knockout mice (*Z*/*Z*). **P* < 0.05; ***P* < 0.01 compared with wild type.

$Phf2^{Z/Z}$ mice because adipose tissue is well known to be involved in glucose metabolism. There was no significant change in the glucose or insulin tolerance tests (Supplementary Fig. 3), suggesting that reduced WAT weight did not affect insulin sensitivity in mice at 5 weeks of age.

PHF2 is necessary for normal adipogenesis. To elucidate the role of PHF2 in adipogenesis, we generated $Phf2^{fl/fl}$;*Cre-ERT2* mice by crossing *Phf2* floxed mice with *Cre-ERT2* mice. Stromal vascular cells (SVCs) were then obtained from $Phf2^{fl/fl}$;*Cre-ERT2* mice or control *Cre-ERT2* mice and treated with 4-hydroxytamoxifen (4-OHT) to induce Cre-mediated excision of *Phf2*. As expected, treatment with 4-OHT efficiently reduced mRNA expression of *Phf2* in $Phf2^{fl/fl}$;*Cre-ERT2* but not in control *Cre-ERT2* mice (Fig. 4*C*). When SVCs were treated with a differentiation cocktail to induce their differentiation into adipocytes, differentiation was impaired in 4-OHT-treated SVCs from $Phf2^{fl/fl}$;*Cre-ERT2* mice as shown by oil red O staining (Fig. 4*A* and *B*). This was also confirmed by decreased expression of adipogenic marker genes in 4-OHT–treated SVCs from $Phf2^{fl/fl}$;*Cre-ERT2* mice (Fig. 4*C*). Next, we generated 3T3-L1 cell lines in which PHF2 was stably knocked down by retrovirus carrying *Phf2*-targeted short hairpin RNA. Infection of retrovirus carrying *shPhf2* successfully decreased the expression of *Phf2* (Fig. 4*F*). In accordance with the results from SVCs, short hairpin RNA-mediated knockdown of *Phf2* resulted in impaired adipogenesis in the 3T3-L1 cell line as assessed by oil red O staining (Fig. 4*D* and *E*) and expression of adipogenic marker genes (Fig. 4*F*).

PHF2 is recruited with CEBPA to the promoter regions of adipogenic genes. The results indicated that PHF2 promoted adipogenesis. Moreover, we show that PHF2 works as a coactivator for several transcription factors through H3K9me2 demethylation (5). Therefore, we hypothesized that PHF2 coactivates transcription factors that promote adipogenesis. Among such transcription factors, PPARG and CEBPA are the master regulators for adipogenesis (21). First, we assessed whether PHF2 could physically interact with PPARG or CEBPA. When transfected into HEK293 cells, FLAG-CEBPA (but not FLAG-PPARG) was coimmunoprecipitated with endogenous PHF2 (Fig. 5*A*). Conversely, FLAG-PHF2 was coimmunoprecipitated with endogenous CEBPA in 3T3-L1 adipocytes (Fig. 5*B*). In accordance with these results, ChIP analysis revealed that PHF2 was recruited to known CEBPRE (CEBP responsive elements) in the promoter regions of *Cebpa*, *Pparg*, and *Fabp4* in differentiated

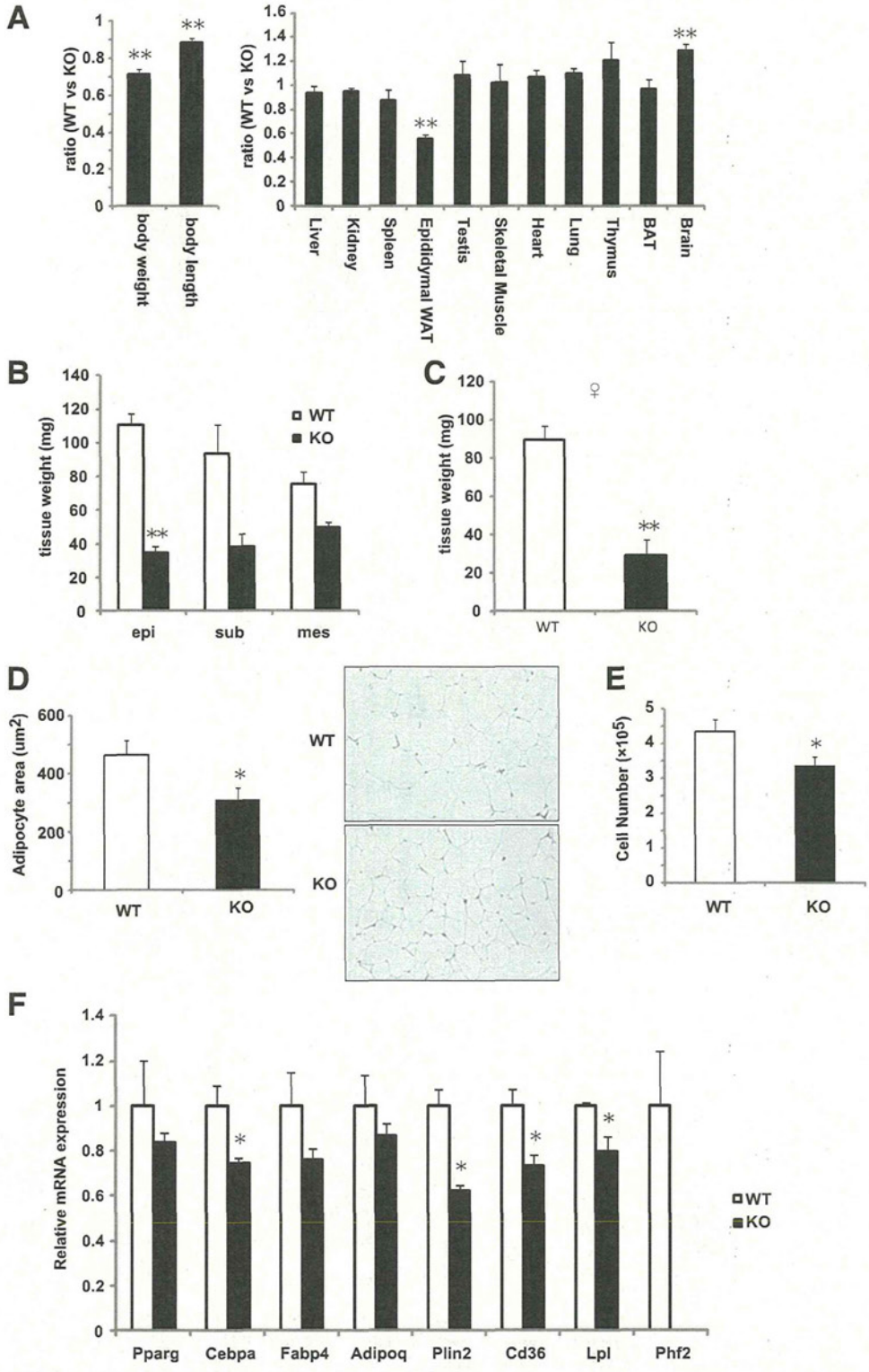

FIG. 3. Assessment of adipose tissue of systemic *Phf2* knockout mice. *A*: Ratio of body weight and nasoanal length or normalized tissue weight of male $Phf2^{Z/Z}$ to WT littermates at 5 weeks of age. Tissue weights were normalized to body weights (n = 6). *B*: Weights of epididymal WAT, subcutaneous WAT, and mesenteric WAT of male $Phf2^{Z/Z}$ KO mice and WT littermates at 5 weeks of age (n = 3). *C*: Weights of gonadal WAT of female $Phf2^{Z/Z}$ KO mice and WT littermates at 5 weeks of age (n = 4). *D*: Mean adipocyte areas of epididymal WAT from $Phf2^{Z/Z}$ KO mice and WT littermates (n = 5). High-magnification micrographs of WAT are shown. *E*: Adipocyte number in epididymal fat pads of $Phf2^{Z/Z}$ KO mice and WT littermates (n = 7). *F*: Real-time qPCR analysis of adipocyte marker genes and *Phf2* of $Phf2^{Z/Z}$ KO mice and WT littermates (n = 3). $^*P < 0.05$; $^{**}P < 0.01$ compared with WT. KO, knockout; WT, wild type. (A high-quality color representation of this figure is available in the online issue.)

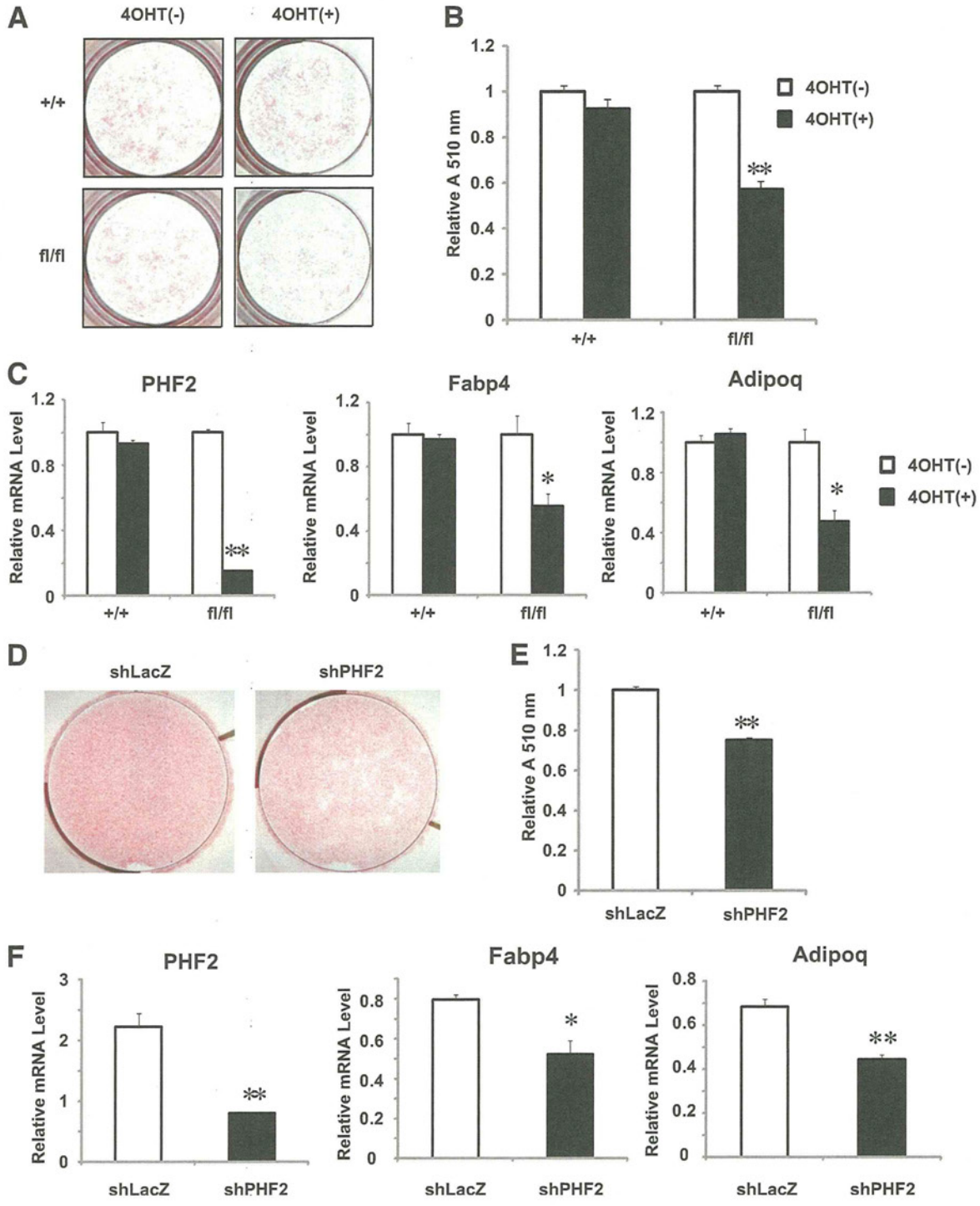

FIG. 4. Effects of PHF2 knock down on adipogenesis. *A–C*: SVCs from *Cre-ERT2; Phf2*$^{fl/fl}$ (*fl/fl*) or *Cre-ERT2* (+/+) were treated with or without 4-OHT and differentiated into adipocytes by treatment with insulin, dexamethasone, and isobutylmethylxanthine. Image (*A*) and quantification (*B*) of oil red O staining and the results of real-time qPCR analysis of adipocyte marker genes (*C*) are shown ($n = 3$). *D–F*: 3T3-L1 cells infected with retroviruses containing either pSuper-retro-shLacZ or pSuper-retro-shPHF2 were differentiated into adipocytes. Image (*D*) and quantification (*E*) of oil red O staining and the results of real-time qPCR analysis of adipocyte marker genes (*F*) are shown ($n = 3$). *$P < 0.05$; **$P < 0.01$ compared with control.

3T3-L1 adipocytes (Fig. 5*C*). These results indicate that PHF2 might work as a coactivator for CEBPA. PHF2 seemed to be necessary for recruitment of CEBPA to chromatin because the recruitment of CEBPA to CEBPRE was impaired in 3T3-L1 in which *Phf2* had been knocked down (Fig. 5*D*). Moreover, modification of H3K9me2 in these CEBPRE was significantly increased in *Phf2* knocked-down 3T3-L1 adipocytes (Fig. 5*E*). These data indicate that PHF2 can play

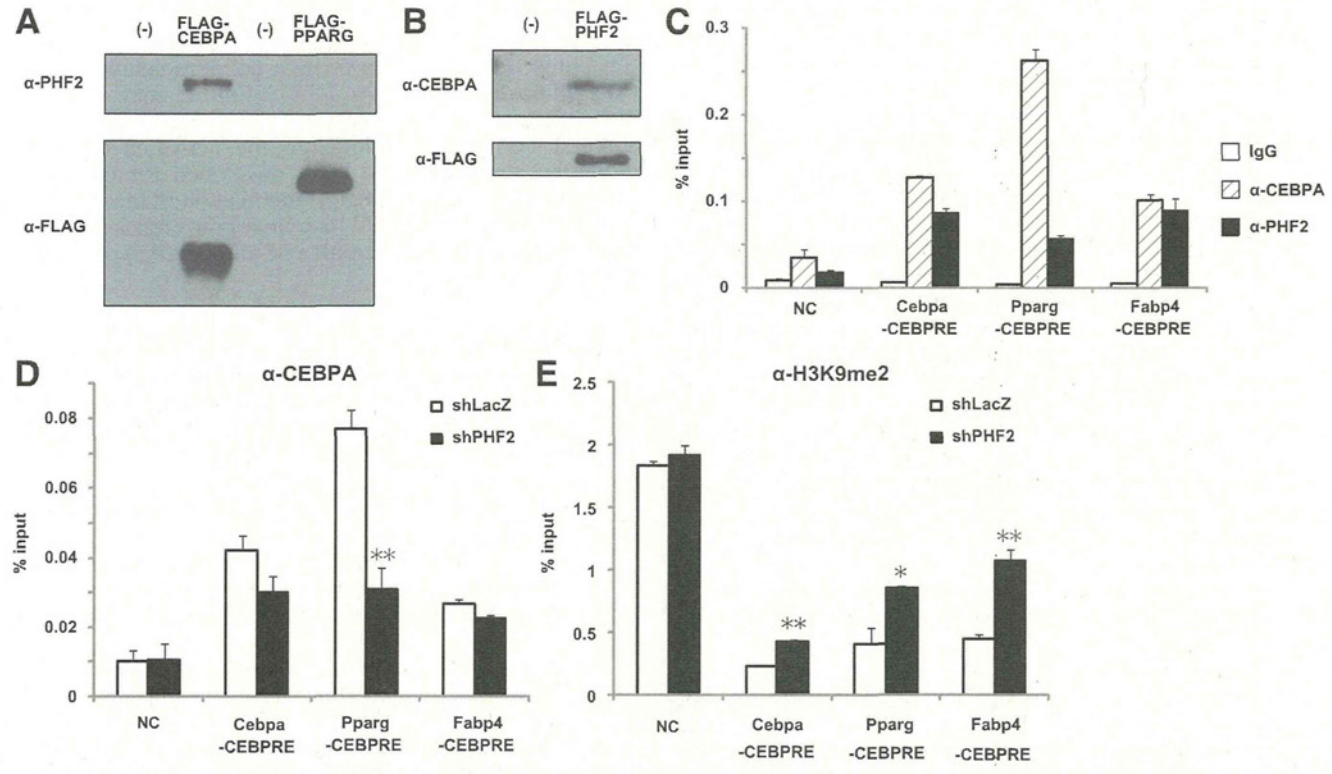

FIG. 5. Association of PHF2 with CEBPA. *A*: **FLAG-CEBPA or FLAG-PPARG was transfected into HEK293T cells. Cells were harvested and immunoprecipitated with anti-FLAG antibody and detected with anti-PHF2 antibody or anti-FLAG antibody.** *B*: **FLAG-PHF2 was transfected into 3T3-L1 adipocytes. Cells were harvested and immunoprecipitated with anti-FLAG antibody and detected with anti-CEBPA antibody or anti-FLAG antibody.** *C*: **3T3-L1 cells were fixed in formaldehyde on day 4 after differentiation, after which chromatin samples were subjected to ChIP analysis with indicated antibodies and amplified with primers toward indicated loci (n = 3).** *D* **and** *E*: **3T3-L1 cells stably transfected with pSuper-retro-shLacZ or pSuper-retro-shPHF2 were differentiated into adipocytes and subjected to ChIP analysis with anti-CEBPA (*D*) or anti-H3K9me2 antibody (*E*), with primers toward the indicated loci (n = 3). *P < 0.05; **P < 0.01 compared with control. NC, negative control region.**

a role as a coactivator, positively regulating adipogenic gene expression with CEBPA through H3K9me2 demethylation near CEBPA-binding regions.

DISCUSSION

To investigate the role of PHF2 in vivo, we generated *Phf2* knockout mice. *Phf2* knockout mice showed partial neonatal death, growth retardation, and reduced body weight. Reduced body weight seems to be mainly related to growth retardation and reduced lean mass in the knockout mice rather than reduced WAT mass because the body weight of *Phf2* knockout mice is still significantly lower than that of wild type at 8 weeks of age (Fig. 2*E*) when the weight of WAT is not different between *Phf2* knockout and wild type (Supplementary Fig. 1). The reason for this phenotype is not clear. PHF2 has been reported to be highly expressed in the neural tube and dorsal root ganglia (22), and *Phf2* represents a candidate gene for hereditary sensory neuropathy type I (HSN1) (23). In fact, the brain weights of *Phf2* knockout mice were larger than wild-type littermates. Taken together, we speculate that *Phf2* knockout mice may exhibit partial neonatal death attributable to defects in the central nervous system. Conditional deletion mutants using brain-specific Cre mice would clarify the precise roles of PHF2 in brain development.

On the other hand, subsequent study revealed that PHF2 plays an important role in adipogenesis. *Phf2* knockout mice produced lipoatrophy in which adipocytes were decreased in size and number. It seemed to be limited to a young age; for example, in *Klf5* knockout mice, atrophic changes in adipose tissue were abolished until 4 weeks of age (20). Although the reduced WAT phenotype in *Phf2* knockout mice disappeared after the mice reached 8 weeks of age and *Phf2* was systemically knocked out in these mice, this phenotype should be the result of a cell-autonomous mechanism because conditional knockout of *Phf2* in primary SVCs obtained from $Phf2^{fl/fl}$;*Cre-ERT* mice resulted in impaired adipogenesis. Moreover, PHF2 interacts with CEBPA, one of the master adipogenic regulators, and is recruited to CEBPRE. In addition, the lipoatrophic changes in *Phf2* knockout mice were stronger in epididymal and subcutaneous WAT than in mesenteric WAT, suggesting that PHF2 may be a possible candidate factor that determines regional variations in adipogenesis reported previously (24). Although adipose tissue is well known to be involved in glucose homeostasis, there was no significant change in glucose metabolism in *Phf2* knockout mice (Supplementary Fig. 3). There are two possible reasons for this result. First, 5 weeks of age is too young to develop insulin resistance, and second, only slight lipoatrophic change was observed in mesenteric WAT, the mass of which is strongly correlated with insulin resistance. It is meaningful to evaluate glucose metabolism of *Phf2* knockout adult mice under the treatment of a high-fat diet to clarify whether PHF2 plays a role in diabetes.

It is well known that factors that increase cAMP, such as isobutylmethylxanthine, strongly accelerate adipogenesis

(25). Elevation of cAMP is known to lead to suppression of Wnt10b (26) and Sp1 (27), induction of C/EBPβ (28), and production of PPARγ ligands (29). Moreover, cAMP signaling is mediated by two major pathways, PKA and Epac (exchange proteins directly activated by cAMP), that synergistically induce adipogenesis (30). However, it is not fully understood how PKA stimulates adipogenesis. PHF2 seems to be one possible candidate because it is reportedly activated through phosphorylation by PKA (5), and the current study shows that PHF2 stimulates adipogenesis. It seems that *Phf2* was not transcriptionally regulated during adipogenesis (Supplementary Fig. 4). However, PHF2 might be activated by PKA-mediated phosphorylation by a cAMP inducer in the adipogenic differentiation cocktail.

On the other hand, the weight reduction of BAT was not observed in *Phf2* knockout mice, although PKA and CEBPA were also reported to be necessary for the development of BAT (31). Recently, it was reported that brown adipocytes were differentiated from Myf5-positive precursor cells, which are more closely related to myoblasts rather than to the white preadipocytes (32). Thus, PHF2 may play a role in white preadipocytes but not in brown preadipocytes or myoblasts because the histone demethylases seem to be involved in differentiation in specific cell types.

PHF2 reportedly interacts with ARID5B, which is necessary for the coactivator function of PHF2 (5). Because phenotypes of systemic *Arid5b* knockout animals have already been reported (33–35), it is worth comparing the phenotypes between *Arid5b* knockout and *Phf2* knockout mice. Of note, most *Arid5b* knockout mice die within 24 h of birth, but some pups survive (33). The surviving *Arid5b* knockout animals show dramatically reduced body weight in neonates and adults. The WAT of *Arid5b* knockout mice weighed less than controls because of a reduction in the amount of lipid per cell. Because the phenotype of *Arid5b* knockout mice is close to that of *Phf2* knockout mice, it is likely that PHF2 and ARID5B work together in multiple organs, including adipose tissue.

Transcriptional control of the adipocyte lineage has been studied extensively (21,36). However, little is known about the role of histone demethylases during adipogenesis, even though several studies have clarified the roles of histone deacetylase HDAC1 (37,38) and HDAC3 (39) and histone demethylase LSD1 (40) in adipogenesis. In the current study, we found that histone demethylase PHF2 plays an important role in adipogenesis in vivo. Notably, several studies reported the role of histone demethylation in cell differentiation; for example, LSD1 controls pituitary terminal cell-type differentiation (6), JMJD3, an H3K27me3 demethylase, potentiates epidermal differentiation (41); and JMJD1A, an H3K9 demethylase, potentiates smooth muscle cell differentiation (42). In general, histone demethylases may play roles in cell differentiation in specific cell types. We suggest that PHF2 may be a significant histone demethylase in adipocytogenesis.

Adipose tissue plays an essential role in energy homeostasis. In mammals, WAT stores excess energy as triglycerides from fatty acids imported from circulating lipoproteins. Moreover, recent studies established adipose tissue as an active endocrine organ that secretes various humoral factors called adipokines that work in various physiological pathways, such as feeding, insulin resistance, inflammation, and atherogenesis (43). Thus, clarifications of precise molecular mechanisms that control adipose tissue development should improve our understanding of the pathogenesis and pathophysiology of the metabolic syndrome, diabetes, and other metabolism-related diseases. In this study, PHF2 appears to be a novel molecule that controls adipogenesis in vivo. Modulation of enzymatic activities has been a good target of small molecules. In fact, some drugs that can modulate the activities of histone-modifying enzymes have been developed for clinical use (44–46). Thus, pharmacological modulation of the histone demethylase activity of PHF2 may be a new target in the treatment of human lipodystrophies or adipocyte hyperplasia in diet-induced obesity.

ACKNOWLEDGMENTS

This work was supported by Grants-in-Aid 22790848 from the Ministry of Education, Culture, Sports, Science and Technology (to Y.O.) and a grant for specially promoted research from the Japan Society for the Promotion of Science (to S.K.).

No potential conflicts of interest relevant to this article were reported.

The funder played no role in the conduct of the study, collection of data, management of the study, analysis of data, interpretation of data, or preparation of the manuscript.

Y.O. wrote the manuscript and analyzed data. F.O., T.M., I.T., S.K., and Y.I. designed the experiments. F.O. and Y.I. reviewed and edited the manuscript. K.I. and J.K. performed the microarray analyses. Y.I. is the guarantor of this work and, as such, had full access to all the data in the study and takes responsibility for the integrity of the data and the accuracy of the data analysis.

The authors thank Yoko Yamamoto, Kazuki Inoue, and Erina Inoue, Laboratory of Epigenetic Skeletal Diseases, Institute of Molecular and Cellular Biosciences, The University of Tokyo, Japan, for technical support in the generation of knockout mice.

REFERENCES

1. Jenuwein T, Allis CD. Translating the histone code. Science 2001;293:1074–1080
2. Klose RJ, Kallin EM, Zhang Y. JmjC-domain-containing proteins and histone demethylation. Nat Rev Genet 2006;7:715–727
3. Shi Y. Histone lysine demethylases: emerging roles in development, physiology and disease. Nat Rev Genet 2007;8:829–833
4. Agger K, Christensen J, Cloos PA, Helin K. The emerging functions of histone demethylases. Curr Opin Genet Dev 2008;18:159–168
5. Baba A, Ohtake F, Okuno Y, et al. PKA-dependent regulation of the histone lysine demethylase complex PHF2-ARID5B. Nat Cell Biol 2011;13:668–675
6. Wang J, Scully K, Zhu X, et al. Opposing LSD1 complexes function in developmental gene activation and repression programmes. Nature 2007;446:882–887
7. Okada Y, Scott G, Ray MK, Mishina Y, Zhang Y. Histone demethylase JHDM2A is critical for *Tnp1* and *Prm1* transcription and spermatogenesis. Nature 2007;450:119–123
8. Tateishi K, Okada Y, Kallin EM, Zhang Y. Role of Jhdm2a in regulating metabolic gene expression and obesity resistance. Nature 2009;458:757–761
9. Qi HH, Sarkissian M, Hu GQ, et al. Histone H4K20/H3K9 demethylase PHF8 regulates zebrafish brain and craniofacial development. Nature 2010;466:503–507
10. Tsukada Y, Ishitani T, Nakayama KI. KDM7 is a dual demethylase for histone H3 Lys 9 and Lys 27 and functions in brain development. Genes Dev 2010;24:432–437
11. Wen H, Li J, Song T, et al. Recognition of histone H3K4 trimethylation by the plant homeodomain of PHF2 modulates histone demethylation. J Biol Chem 2010;285:9322–9326
12. Lee EC, Yu D, Martinez de Velasco J, et al. A highly efficient *Escherichia coli*-based chromosome engineering system adapted for recombinogenic targeting and subcloning of BAC DNA. Genomics 2001;73:56–65

13. Dupé V, Davenne M, Brocard J, et al. In vivo functional analysis of the Hoxa-1 3′ retinoic acid response element (3′RARE). Development 1997; 124:399–410
14. Ruzankina Y, Pinzon-Guzman C, Asare A, et al. Deletion of the developmentally essential gene *ATR* in adult mice leads to age-related phenotypes and stem cell loss. Cell Stem Cell 2007;1:113–126
15. Iwaki M, Matsuda M, Maeda N, et al. Induction of adiponectin, a fat-derived antidiabetic and antiatherogenic factor, by nuclear receptors. Diabetes 2003;52:1655–1663
16. Ohtake F, Baba A, Takada I, et al. Dioxin receptor is a ligand-dependent E3 ubiquitin ligase. Nature 2007;446:562–566
17. Kanno J, Aisaki K, Igarashi K, et al. "Per cell" normalization method for mRNA measurement by quantitative PCR and microarrays. BMC Genomics 2006;7:64
18. Mersmann HJ, MacNeil MD. Variables in estimation of adipocyte size and number with a particle counter. J Anim Sci 1986;62:980–991
19. Ramírez-Zacarías JL, Castro-Muñozledo F, Kuri-Harcuch W. Quantitation of adipose conversion and triglycerides by staining intracytoplasmic lipids with Oil red O. Histochemistry 1992;97:493–497
20. Oishi Y, Manabe I, Tobe K, et al. Krüppel-like transcription factor KLF5 is a key regulator of adipocyte differentiation. Cell Metab 2005;1:27–39
21. Farmer SR. Transcriptional control of adipocyte formation. Cell Metab 2006;4:263–273
22. Hasenpusch-Theil K, Chadwick BP, Theil T, Heath SK, Wilkinson DG, Frischauf AM. PHF2, a novel PHD finger gene located on human chromosome 9q22. Mamm Genome 1999;10:294–298
23. Nicholson GA, Dawkins JL, Blair IP, et al. The gene for hereditary sensory neuropathy type I (HSN-I) maps to chromosome 9q22.1-q22.3. Nat Genet 1996;13:101–104
24. Tchkonia T, Giorgadze N, Pirtskhalava T, et al. Fat depot origin affects adipogenesis in primary cultured and cloned human preadipocytes. Am J Physiol Regul Integr Comp Physiol 2002;282:R1286–R1296
25. Yarwood SJ, Anderson NG, Kilgour E. Cyclic AMP modulates adipogenesis in 3T3-F442A cells. Biochem Soc Trans 1995;23:175S
26. Bennett CN, Ross SE, Longo KA, et al. Regulation of Wnt signaling during adipogenesis. J Biol Chem 2002;277:30998–31004
27. Tang QQ, Jiang MS, Lane MD. Repressive effect of Sp1 on the C/EBPalpha gene promoter: role in adipocyte differentiation. Mol Cell Biol 1999;19: 4855–4865
28. Yeh WC, Cao Z, Classon M, McKnight SL. Cascade regulation of terminal adipocyte differentiation by three members of the C/EBP family of leucine zipper proteins. Genes Dev 1995;9:168–181
29. Tzameli I, Fang H, Ollero M, et al. Regulated production of a peroxisome proliferator-activated receptor-gamma ligand during an early phase of adipocyte differentiation in 3T3-L1 adipocytes. J Biol Chem 2004;279: 36093–36102
30. Petersen RK, Madsen L, Pedersen LM, et al. Cyclic AMP (cAMP)-mediated stimulation of adipocyte differentiation requires the synergistic action of Epac- and cAMP-dependent protein kinase-dependent processes. Mol Cell Biol 2008;28:3804–3816
31. Wang ND, Finegold MJ, Bradley A, et al. Impaired energy homeostasis in C/EBP alpha knockout mice. Science 1995;269:1108–1112
32. Seale P, Bjork B, Yang W, et al. PRDM16 controls a brown fat/skeletal muscle switch. Nature 2008;454:961–967
33. Whitson RH, Tsark W, Huang TH, Itakura K. Neonatal mortality and leanness in mice lacking the ARID transcription factor Mrf-2. Biochem Biophys Res Commun 2003;312:997–1004
34. Lahoud MH, Ristevski S, Venter DJ, et al. Gene targeting of Desrt, a novel ARID class DNA-binding protein, causes growth retardation and abnormal development of reproductive organs. Genome Res 2001;11:1327–1334
35. Schmahl J, Raymond CS, Soriano P. PDGF signaling specificity is mediated through multiple immediate early genes. Nat Genet 2007;39:52–60
36. MacDougald OA, Lane MD. Transcriptional regulation of gene expression during adipocyte differentiation. Annu Rev Biochem 1995;64:345–373
37. Wiper-Bergeron N, Wu D, Pope L, Schild-Poulter C, Haché RJ. Stimulation of preadipocyte differentiation by steroid through targeting of an HDAC1 complex. EMBO J 2003;22:2135–2145
38. Yoo EJ, Chung JJ, Choe SS, Kim KH, Kim JB. Down-regulation of histone deacetylases stimulates adipocyte differentiation. J Biol Chem 2006;281: 6608–6615
39. Fajas L, Egler V, Reiter R, et al. The retinoblastoma-histone deacetylase 3 complex inhibits PPARgamma and adipocyte differentiation. Dev Cell 2002;3:903–910
40. Musri MM, Carmona MC, Hanzu FA, Kaliman P, Gomis R, Párrizas M. Histone demethylase LSD1 regulates adipogenesis. J Biol Chem 2010;285: 30034–30041
41. Sen GL, Webster DE, Barragan DI, Chang HY, Khavari PA. Control of differentiation in a self-renewing mammalian tissue by the histone demethylase JMJD3. Genes Dev 2008;22:1865–1870
42. Lockman K, Taylor JM, Mack CP. The histone demethylase, Jmjd1a, interacts with the myocardin factors to regulate SMC differentiation marker gene expression. Circ Res 2007;101:e115–e123
43. Flier JS. Obesity wars: molecular progress confronts an expanding epidemic. Cell 2004;116:337–350
44. McCabe MT, Ott HM, Ganji G, et al. EZH2 inhibition as a therapeutic strategy for lymphoma with EZH2-activating mutations [letter to the editor online], 2012. Available from http://www.nature.com/nature/journal/vaop/ncurrent/full/nature11606.html. Accessed 2 November 2012
45. Song SH, Han SW, Bang YJ. Epigenetic-based therapies in cancer: progress to date. Drugs 2011;71:2391–2403
46. Tan J, Cang S, Ma Y, Petrillo RL, Liu D. Novel histone deacetylase inhibitors in clinical trials as anti-cancer agents. J Hematol Oncol 2010;3:5

Reproductive Toxicology 34 (2012) 93–100

Contents lists available at SciVerse ScienceDirect

Reproductive Toxicology

journal homepage: www.elsevier.com/locate/reprotox

Increased cellular distribution of vimentin and Ret in the cingulum induced by developmental hypothyroidism in rat offspring maternally exposed to anti-thyroid agents

Hitoshi Fujimoto[a], Gye-Hyeong Woo[a], Kaoru Inoue[a], Katsuhide Igarashi[b], Jun Kanno[b], Masao Hirose[c], Akiyoshi Nishikawa[d], Makoto Shibutani[a,e,*]

[a] Division of Pathology, National Institute of Health Sciences, 1–18–1 Kamiyoga, Setagaya-ku, Tokyo 158-8501, Japan
[b] Division of Molecular Toxicology, National Institute of Health Sciences, 1–18–1 Kamiyoga, Setagaya-ku, Tokyo 158-8501, Japan
[d] Biological Safety Research Center, National Institute of Health Sciences, 1–18–1 Kamiyoga, Setagaya-ku, Tokyo 158-8501, Japan
[c] Food Safety Commission, 5–2–20 Akasaka Park Bld. 22nd Floor, Akasaka, Minato-ku, Tokyo 107-6122, Japan
[e] Laboratory of Veterinary Pathology, Tokyo University of Agriculture and Technology, 3–5–8 Saiwai-cho, Fuchu-shi, Tokyo 183-8509, Japan

ARTICLE INFO

Article history:
Received 4 December 2011
Received in revised form 19 February 2012
Accepted 16 March 2012
Available online 6 April 2012

Keywords:
Developmental hypothyroidism
Cerebral white matter
Vimentin
Ret
Rat

ABSTRACT

To elucidate target molecules of white matter development responding to hypothyroidism, global gene expression profiling of cerebral white matter from male rat offspring was performed after maternal exposure to anti-thyroid agents, 6-propyl-2-thiouracil and methimazole, on postnatal day 20. Genes involved in central nervous system development commonly up- or down-regulated among groups treated with anti-thyroid agents. Immunohistochemical distributions of vimentin, Ret proto-oncogene (Ret), deleted in colorectal cancer protein (DCC), and Claudin11 (Cld11) were examined based on the gene expression profile. Immunoreactive cells for vimentin and Ret in the cingulum, and the immunoreactive intensity of Cld11 and DCC in whole white matter were increased by treatment with anti-thyroid agents. Immunoreactive cells for vimentin and Ret were immature astrocytes and oligodendrocytes, respectively. Thus, immunoreactive cells for vimentin and Ret may be quantitatively measurable targets of developmental hypothyroidism in white matter.

1. Introduction

Thyroid hormones are essential for normal fetal and neonatal brain development, control neuronal and glial proliferation in definitive brain regions and regulate neuronal migration and differentiation [1–3]. In humans, maternal hypothyroxinemia early in pregnancy may adversely affect fetal brain development, and importantly, even mild to moderate hypothyroxinemia may result in suboptimal neurodevelopment [4], thereby increasing the concern of impaired brain development induced by exposure to thyroid hormone-disrupting chemicals in the environment.

Developmental hypothyroidism leads to growth retardation, neurological defects and impaired performance in various behavioral learning actions [5,6]. Rat offspring maternally exposed to anti-thyroid agents, such as 6-propyl-2-thiouracil (PTU) and methimazole (MMI), show impaired brain growth including white matter hypoplasia with decreased axonal myelination and oligodendrocytes, and impairment of neurogenesis, neuronal migration, dendritic arborization and synapse formation [2,7–9]. These types of impaired brain growth are permanent and accompanied by apparent structural and functional abnormalities. However, the molecular mechanism of impaired brain growth is still unclear.

Histological lesion-specific gene expression profiling provides valuable information on the mechanisms underlying lesion development. In previous studies, we established molecular analysis methods for DNA, RNA and proteins in paraffin-embedded small tissue specimens using the organic solvent-based fixative methacarn, with high performance similar to that of unfixed frozen tissue specimens [10–12]. These methods have been used to analyze global gene expression changes in microdissected lesions [13–15].

Abbreviations: CC, corpus callosum; Cld11, claudin 11; CNS, central nervous system; DCC, deleted in colorectal cancer protein; GAPDH, glyceraldehyde 3-phosphate dehydrogenase; GD, gestation day; GDNF, glial cell line-derived neurotrophic factor; GFAP, glial fibrillary acidic protein; MMI, methimazole; OSP, oligodendrocyte specific protein; PCR, polymerase chain reaction; PND, postnatal day; PTU, 6-propyl-2-thiouracil; Ret, Ret proto-oncogene; RT, reverse transcription; v-Maf, v-maf musculoaponeurotic fibrosarcoma oncogene; Zfhx1b, zinc finger homeobox 1b.

* Corresponding author at: Laboratory of Veterinary Pathology, Tokyo University of Agriculture and Technology, 3–5–8 Saiwai-cho, Fuchu-shi, Tokyo 183-8509, Japan. Tel.: +81 42 367 5874; fax: +81 42 367 5771.
E-mail address: mshibuta@cc.tuat.ac.jp (M. Shibutani).

0890-6238/$ – see front matter © 2012 Elsevier Inc. All rights reserved.
http://dx.doi.org/10.1016/j.reprotox.2012.03.005

To evaluate in vivo developmental brain growth effects of thyroid hormone-disrupting chemicals, we morphometrically analyzed neuronal migration and white matter development in a rat developmental hypothyroidism model [16]. Molecules involved in aberrant neurogenesis and neuronal mismigration were identified by global gene expression analysis of the hippocampal area [15]. In the present study, to elucidate marker molecules in white matter involved in developmental hypothyroidism, we performed global gene expression profiling using microarrays. To obtain the white matter-specific gene expression profile, a microdissection technique was applied to the corpus callosum (CC) and bilateral cerebral white matter. Based on expression profiles, cellular localization of selected molecules was then immunohistochemically examined in cerebral white matter after developmental exposure to anti-thyroid agents.

2. Materials and methods

2.1. Chemicals and animals

6-propyl-2-thiouracil (PTU; CAS No. 51-52-9) and methimazole (MMI; CAS No. 60-56-0) were purchased from Sigma Chemical Co. (St. Louis, MO). Pregnant CD® (SD) IGS rats at gestational day (GD) 3 (GD 0: the day vaginal plugs appeared) were purchased from Charles River Japan Inc. (Yokohama, Japan). Animals were individually housed in polycarbonate cages (SK-Clean, 41.5 cm × 26 cm × 17.5 cm; CLEA Japan Inc., Tokyo, Japan) with wood chip bedding (Sankyo Lab Service Corp., Tokyo, Japan) and maintained in a climate-controlled animal room (24 ± 1 °C, relative humidity: 55 ± 5%) with a 12 h light/dark cycle. A soy-free diet (Oriental Yeast Co. Ltd., Tokyo, Japan) was chosen as the basal diet for maternal animals to eliminate possible phytoestrogen effects [17]. Animals received food and water ad libitum throughout experimentation including a 1 week acclimation period.

2.2. Experimental design

Animal experiments are described elsewhere [16]. Briefly, maternal animals were randomly divided into four groups including an untreated control. Eight dams per group were treated with 3 or 12 ppm PTU or 200 ppm MMI, which was added to drinking water from GD 10 to postnatal day (PND) 20 (PND 0: the day of delivery). On PND 2, four male and four female offspring per dam were randomly selected and remaining litters were culled. On PND 20, 20 male and 20 female offspring (at least one male and one female per dam) per group were subjected to prepubertal necropsy [16,18]. All animals were weighed and sacrificed by exsanguination from the abdominal aorta under deep anesthesia with ether. Animal protocols were reviewed and approved by the Animal Care and Use Committee of the National Institute of Health Sciences, Japan.

2.3. Preparation of tissue specimens and microdissection

For microarray and real-time reverse transcription (RT)-polymerase chain reaction (PCR) analyses, the whole brain of male offspring was immediately removed at prepubertal necropsy on PND 20 ($n = 4$/group) and fixed with methacarn solution for 2 h at 4 °C [10]. Coronal brain slices taken at −3.5 mm from the bregma were dehydrated and embedded in paraffin. Embedded tissues were stored at 4 °C until tissue sectioning for microdissection [19].

For microdissection, 4 and 20 μm-thick serial sections were prepared. The 4 μm-thick sections were stained with hematoxylin and eosin for confirmation of anatomical orientation of the hippocampal substructure to aid microdissection (Fig. 1). The 20 μm-thick sections were mounted onto PEN-foil film (Leica Microsystems GmbH, Welzlar, Germany) overlaid on glass slides, dried in an incubator overnight at 37 °C, and then stained using an LCM staining kit (Ambion, Inc., Austin, TX). Regions of CC and bilateral cerebral white matter (external capsule) in sections, as shown in Fig. 1, were subjected to laser microbeam microdissection (Leica Microsystems GmbH). Forty sections from each animal were used for microdissection, and microdissected samples were individually stored in 1.5 ml tubes at −80 °C until total RNA extraction.

2.4. RNA preparation, amplification and microarray analysis

Total RNA extraction from microdissected regions, quantitation of RNA yield, and RNA amplification were performed using methods described elsewhere [14,15,19].

For microarray analysis, second-round-amplified biotin-labeled antisense RNAs were subjected to hybridization with a GeneChip® Rat Genome 230 2.0 Array (Affymetrix, Inc., Santa Clara, CA).

Gene selection and normalization of expression data were performed using GeneSpring® software 7.2 (Silicon Genetics, Redwood City, CA). Per chip normalization was performed according to a method described elsewhere [14,15]. Genes with expression changes of at least 2-fold in magnitude compared with those of untreated controls were selected. Common genes with altered expression in anti-thyroid agent exposed groups were also selected.

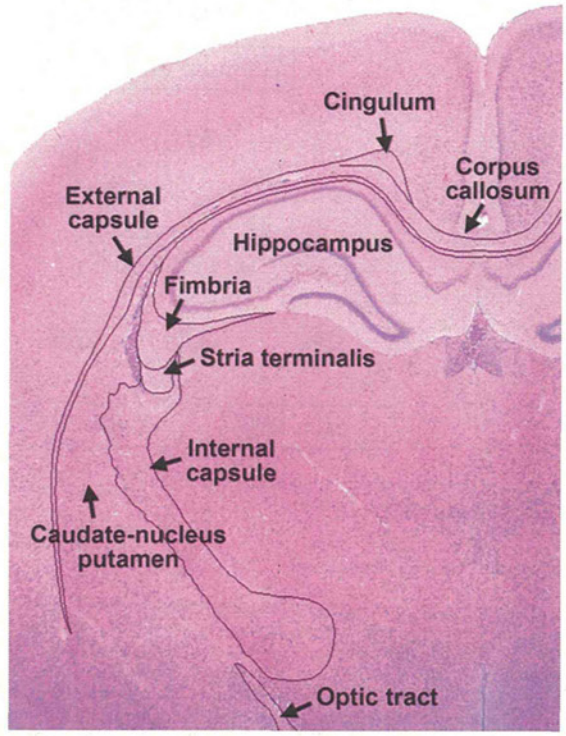

Fig. 1. Overview of the cerebral hemisphere of a male rat at PND 20 stained with hematoxylin and eosin. Magnification, 12.5×.

2.5. Real-time RT-PCR

Quantitative real-time RT-PCR using an ABI Prism 7900HT (Applied Biosystems Japan Ltd., Tokyo, Japan) was performed for confirmation of expression values obtained from microarray analysis. Selected genes showed altered expression (≥2-fold, ≤0.5-fold) in any of the anti-thyroid agent-exposed animals as compared with those of untreated controls. For example, vimentin, *Ret*, v-maf musculoaponeurotic fibrosarcoma oncogene (*v-Maf*) and tektin 4 as up-regulated genes, and *Cld11* and zinc finger homeobox 1b (*Zfhx1b*) as down-regulated ones. RT was performed using first-round antisense RNAs prepared for microarray analysis. For real-time PCR analysis, ABI Assays-on-Demand™ TaqMan® probe and primer sets from Applied Biosystems ($n = 4$/group) were used. For quantification of expression data, a standard curve method was applied. Expression values were normalized to glyceraldehyde 3-phosphate dehydrogenase (GAPDH) using TaqMan® Rodent GAPDH Control Reagents (Applied Biosystems Japan Ltd.).

2.6. Immunohistochemistry

To evaluate the immunohistochemical distribution of molecules identified by microarray analysis, the brains of male pups obtained at PND 20 were fixed in Bouin's solution at room temperature overnight. Ten animals for each group were used except for the untreated control group with six animals.

Antibodies against vimentin (mouse monoclonal antibody, 1:200; Millipore Corporation, Billerica, MA), glial fibrillary acidic protein (GFAP, rabbit polyclonal antibody, 1:500; Dako, Glostrup, Denmark), Ret (rabbit polyclonal antibody, 1:50; Santa Cruz Biotechnology, Inc., Santa Cruz, CA), DCC (mouse monoclonal antibody, 1:40; Leica Microsystems GmbH), and oligodendrocyte specific protein (OSP, same as Cld11, rabbit polyclonal antibody, 1:200; Novus Biologicals, Inc., Co., Littleton, CO) were used for immunohistochemistry. For antigen retrieval, sections were heated in 10 mM citrate buffer in a microwave for 10 min before incubation with anti-vimentin and -DCC antibodies. Immunodetection was carried out using a VECTASTAIN® Elite ABC kit (Vector Laboratories Inc., Burlingame, CA) with 3,3′-diaminobenzidine/H_2O_2 for the chromogen as described elsewhere [13,14]. Sections were then counterstained with hematoxylin and coverslipped for microscopic examination.

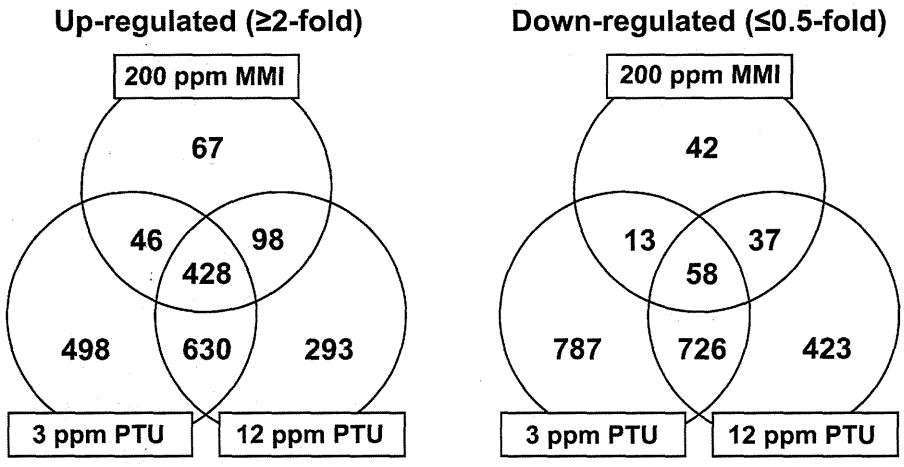

Fig. 2. Venn diagram of genes with altered expression in microarray analysis in response to maternal exposure to anti-thyroid agents. (Left) Up-regulated genes (≥2-fold). (Right) Down-regulated genes (≤0.5-fold).

2.7. Morphometry of immunolocalized cells

The number of immunoreactive cells was quantitatively measured by vimentin and Ret expression in white matter at the cingulum of the bilateral sides using two sections with an approximately 100 μm interval (i.e. four images per animal; Fig. 1), and values were normalized and expressed as those in the unit area (cm^2). GFAP-immunoreactive cells were similarly measured. For quantitative measurement of each immunoreactive cellular component containing vimentin, Ret and GFAP, digital photomicrographs at 100-fold magnification were taken using a BX51 microscope (Olympus Optical Co., Ltd., Tokyo, Japan) attached to a DP70 Digital Camera System (Olympus Optical Co.), and quantitative measurements were performed using WinROOF image analysis software 5.7 (Mitani Corp., Fukui, Japan). To evaluate immunoreactivity of DCC and Cld11 in white matter, staining intensity was scored as 0 (none), 1 (minimal), 2 (slight), 3 (moderate) and 4 (strong) by observation at 40-fold magnification.

2.8. Statistical analysis

Numerical data were assessed by one-way analysis of variance or the Kruskal–Wallis test following Bartlett's test. Statistically significant differences were analyzed by Dunnett's multiple test for comparison with that of the untreated control group. For grading immunohistochemical findings, scores of DCC and Cld11 expression were analyzed with the Mann-Whitney's *U*-test between the untreated control group and each anti-thyroid agent treated group.

3. Results

3.1. Global gene expression analysis

Fig. 2 shows the Venn diagram of genes with altered expression in microdissected cerebral white matter in treated groups in combination or individually in each treated group. Numerous common genes were found to be up- or down-regulated in two of the three treatment groups. The number of genes with up- or down-regulation in response to 3 ppm PTU was higher compared with that of 12 ppm PTU. The number of genes with

Table 1
List of representative genes associated with brain development showing up- or down-regulation common to treatments with MMI and PTU at both 3 and 12 ppm (≥2-fold, ≤0.5-fold).

Accession no.	Gene title	Symbol	MMI	PTU, 3 ppm	PTU, 12 ppm
Up-regulated (20 genes)					
NM_052803	ATPase, Cu++ transporting, alpha polypeptide	*Atp7a*	5.02	11.39	11.09
NM_001108322	T-box 1	*Tbx1*	4.20	4.34	2.31
NM_001191609	Laminin, alpha 5	*Lama5*	4.11	11.57	9.35
NM_031550	Cyclin-dependent kinase inhibitor 2A	*Cdkn2a*	3.59	2.70	3.37
NM_001114330	Glutamate receptor, metabotropic 1	*Grm1*	3.45	2.92	5.89
(NM_001114330)			(3.01)	(2.85)	(2.88)
NM_023091	gamma-Aminobutyric acid A receptor, epsilon	*Gabre*	3.20	3.91	7.46
NM_001107692	Ephrin A4	*Efna4*	3.13	5.07	6.72
NM_001002805	Complement component 4a	*C4a*	3.04	7.15	6.43
NM_019328	Nuclear receptor subfamily 4, group A, member 2	*Nr4a2*	2.97	2.87	4.92
NM_001110099	Ret proto-oncogene	*Ret*	2.89	5.01	4.39
NM_053629	Follistatin-like 3	*Fstl3*	2.85	4.28	6.08
NM_053708	Gastrulation brain homeobox 2	*Gbx2*	2.82	4.73	4.09
NM_019236	Hairy and enhancer of split 2	*Hes2*	2.76	2.93	3.11
NM_001109223	Wingless-related MMTV integration site 16	*Wnt16*	2.71	2.42	3.82
XM_001077495	Nuclear receptor co-repressor 1	*Ncor1*	2.67	2.01	2.97
NM_001012220	Cation channel, sperm associated 2	*Catsper2*	2.54	6.69	4.56
NM_001024275	Ras association (RalGDS/AF-6) domain family 4	*Rassf4*	2.31	4.67	5.43
NM_138900	Complement component 1, s subcomponent	*C1s*	2.12	3.31	3.88
NM_031140	Vimentin	*Vim*	2.11	6.01	4.27
NM_053555	Vesicle-associated membrane protein 5	*Vamp5*	2.04	2.62	3.41
Down-regulated (4 genes)					
NM_013107	Bone morphogenetic protein 6	*Bmp6*	0.23	0.38	0.25
NM_053759	Sine oculis homeobox homolog 1	*Six1*	0.45	0.35	0.46
NM_019280	Gap junction membrane channel protein alpha 5	*Gja5*	0.46	0.16	0.28
NM_133293	GATA binding protein 3	*Gata3*	0.47	0.47	0.24

Abbreviations: MMI, 2-mercapto-1-methylimidazole; PTU, 6-propyl-2-thiouracil.

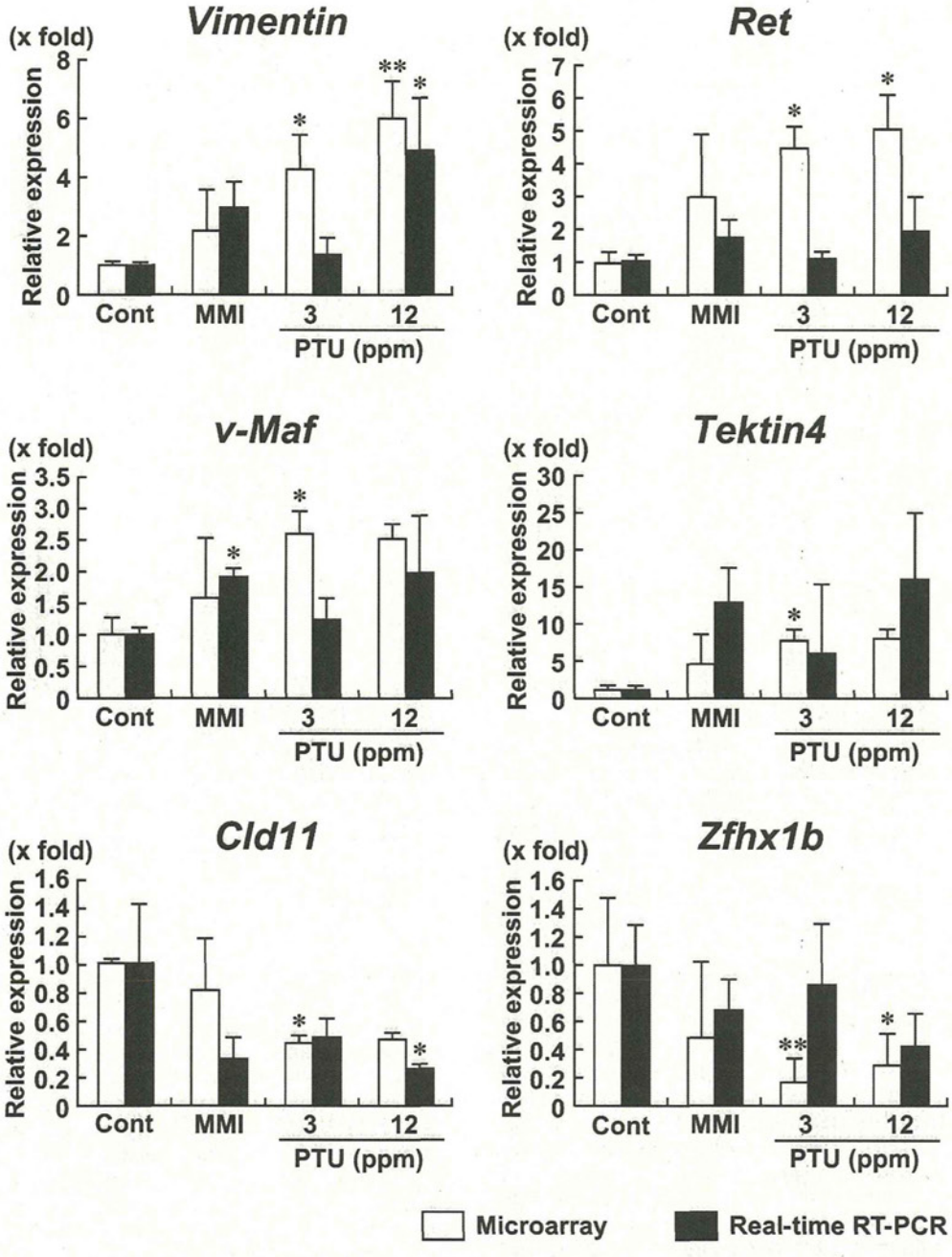

Fig. 3. Validation of mRNA expression of genes selected from microarray data ($n = 4$ in each group). $^{*}P < 0.05$, $^{**}P < 0.01$ vs. untreated controls.

up- or down-regulation in response to 200 ppm MMI was much lower compared with those of both PTU groups. Four hundred and eighty six common genes (428 up-regulated; 58 down-regulated) were identified with altered expression between MMI and both PTU groups (Fig. 2 and Supplementary data: Tables 1 and 2). Among these genes, the genes associated with central nervous system (CNS) development, cell differentiation and cell adhesion were commonly up- or down-regulated in response to anti-thyroid agents (Supplementary data: Tables 1 and 2). Twenty-four genes (20 up-regulated; 4 down-regulated) were related to CNS development involving glial cell differentiation, axon guidance, myelination, and cellular migration (Table 1). Among them, 12 up-regulated genes and two down-regulated genes showed PTU dose-dependent expression changes. For confirmation of microarray data, four genes that were up-regulated and two genes that were down-regulated in response to anti-thyroid agents were selected for mRNA expression analysis by real-time RT-PCR. Results are summarized in Fig. 3. All genes examined showed fluctuations in transcript levels in any of anti-thyroid agent treatment groups, which was similar to that of microarray data.

3.2. Immunolocalization of selected molecules in cerebral white matter

Immunohistochemical localization of vimentin, Ret, DCC and Cld11 was examined in the cerebral white matter. Within white

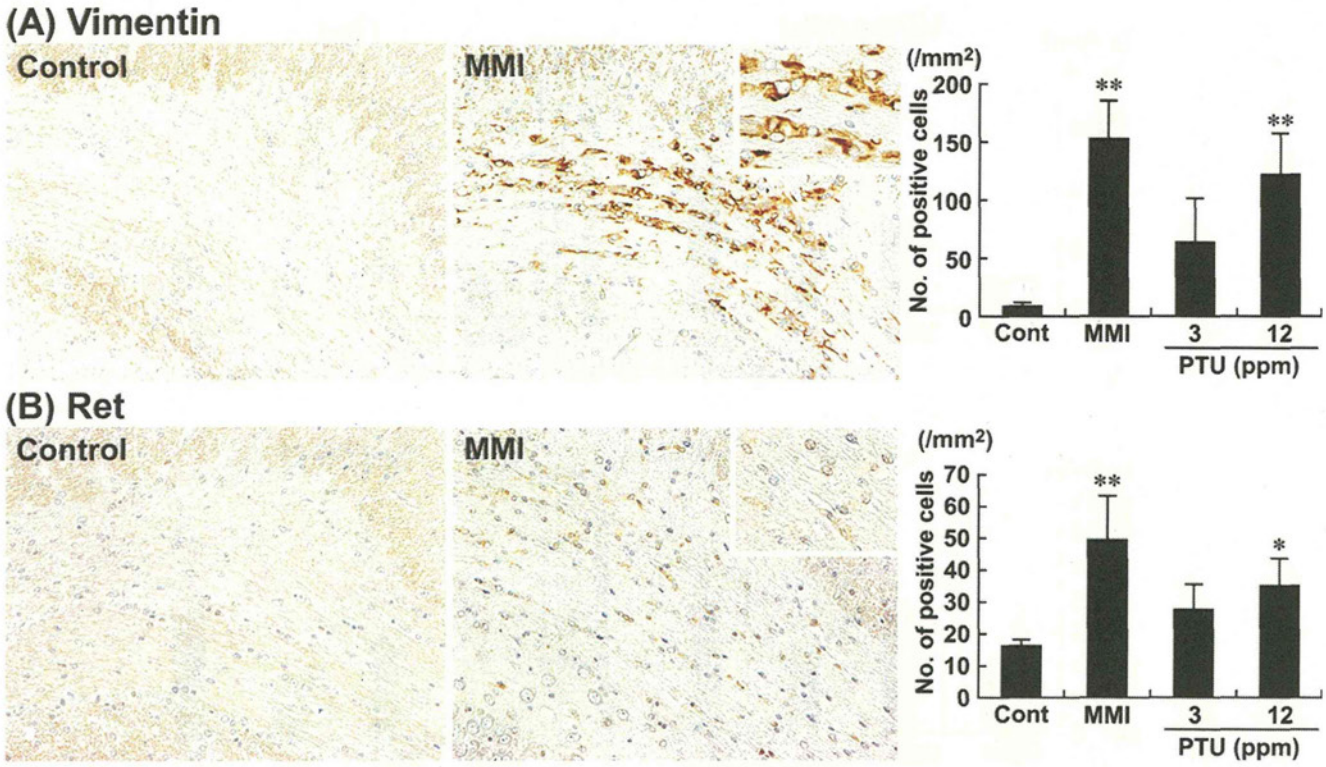

Fig. 4. Immunohistochemical distributions of vimentin- and Ret-positive cells in the while matter tissue. (A) Vimentin-immunoreactive cells in the cingulum. Untreated control animal (left) and MMI-treated animal (right). 200× magnification (inset: 400× magnification). Graph shows the mean number of positive cells within the cingulum at 200× magnification (untreated controls: $n = 6$; MMI and PTU groups: $n = 10$). $^{**}P < 0.01$ vs. untreated controls. (B) Ret-immunoreactive cells in the cingulum. Untreated control animal (left), MMI-treated animal (right). 200× magnification (inset: 400× magnification). Graph shows the mean number of positive cells within the cingulum at 100× magnification (untreated controls: $n = 6$; MMI and PTU groups: $n = 10$). $^{*}P < 0.05$, $^{**}P < 0.01$ vs. untreated controls.

matter tissues, vimentin-immunoreactive cells were scarcely distributed in untreated control animals (Fig. 4A). After treatment with anti-thyroid agents, the distribution of vimentin-positive cells were mainly observed in the cingulum with a statistically significant increase in number with MMI and 12 ppm PTU treatments (Fig. 4A).

Ret-immunoreactive cells were mainly observed in white matter tissues of untreated control animals (Fig. 4B). After treatment with anti-thyroid agents, Ret-positive cells were mainly observed in the cingulum with a statistically significant increase in number with MMI and 12 ppm PTU treatments (Fig. 4B).

DCC showed diffuse immunoreactivity in white matter, indicating myelin sheaths with a statistically significant increase in the intensity scores of animals treated with MMI and 12 ppm PTU as compared with those of the untreated control (Fig. 5A).

Diffuse Cld11-immunoreactivity was observed in white matter, indicating myelin sheaths (Fig. 5B). The immunoreactivity showed a statistically significant increase in the intensity score of animals treated with MMI as compared with that of the untreated control (Fig. 5B).

3.3. *Immunolocalization of GFAP*

To investigate the cell type of vimentin-positive cells, cellular distribution of GFAP immunoreactivity was analyzed as a marker of astrocytes. Untreated control animals showed scattered distribution of GFAP-immunoreactive cells in cerebral white matter, and the number of GFAP-immunoreactive cells was higher compared with that of vimentin-positive cells. GFAP-immunoreactive cells showed a similar distribution to that of vimentin-immunoreactive cells, with accumulated distribution in the cingulum (Fig. 6). After treatment with anti-thyroid agents, the number of GFAP-positive cells was significantly increased in animals treated with MMI and 12 ppm PTU.

4. Discussion

In our previous study [16], maternal exposure to MMI and PTU induced typical hypothyroidism-related changes in the concentration of thyroid-related hormones, and variability in the distribution of hippocampal CA1 pyramidal neurons due to neuronal mismigration [16]. With regard to thyroid hormone-related changes in functions or structures in glial cell populations, gene expression alternations have been reported in myelin-related protein genes related to oligodendrocytes [20,21], as well as in enzymes or cytoskeletal components related to astrocytes [22–24]. Therefore, both oligodendrocytes and astrocytes could also be the target of developmental hypothyroidism. We, in the above-mentioned study [16], also observed changes in white matter structures with hypoplasia due to impaired oligodendroglial development as previously reported [2,9]. Using the same study samples, we, in the present study, analyzed immunohistochemical distribution of molecules that showed fluctuations in gene expression from microarray analysis of cerebral white matter tissue collected using microdissection targeting oligodendrocytes and astrocytes. This is the first report to use microarray analysis of gene expression changes induced by developmental hypothyroidism in white matter, whereas there have been such approaches for the study of cerebral cortex and hippocampal substructures [15,25,26]. We found that anti-thyroid agents caused fluctuations in a number of genes associated with CNS development involving glial cell differentiation, axon guidance, myelination, and cellular migration as listed in Table 1. Among them, vimentin, Ret, DCC and Cld11

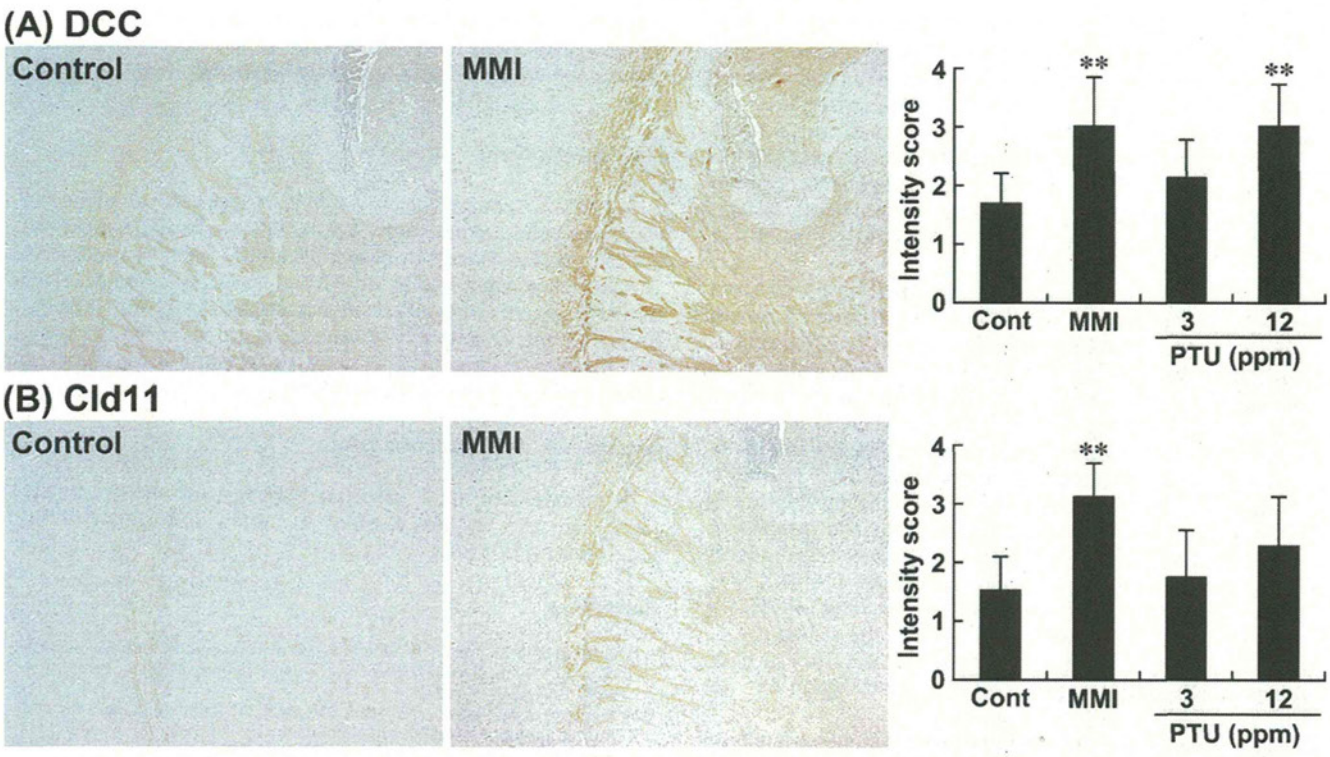

Fig. 5. Immunohistochemical distributions of DCC- and Cld11 in the while matter tissue. (A) DCC-immunoreactivity in the myelin sheath of the external capsule, internal capsule, and fimbria of the hippocampus. Untreated control animal (left), MMI-treated animal (right). 40× magnification. Graph shows the mean intensity score of immunoreactivity at 40× magnification (untreated controls: $n = 6$; MMI and PTU groups: $n = 10$). $^{**}P < 0.01$ vs. untreated controls. (B) Cld11-immunoreactivity in the myelin sheath of the external capsule, internal capsule, and fimbria of the hippocampus. Untreated control animal (left), MMI-treated animal (right). 40× magnification. Graph shows the mean intensity score of immunoreactivity at 40× magnification (untreated controls: $n = 6$; MMI and PTU groups: $n = 10$). $^{**}P < 0.01$ vs. untreated controls.

showed immunohistochemical distribution changes in the cerebral white matter of offspring after maternal exposure to PTU and MMI.

Cld11 is a four-transmembrane protein, which is primarily expressed in oligodendrocytes of the CNS and is the third most abundant CNS myelin protein [27–29]. Cld11 is involved in the formation of intramembranous tight junctions within the myelin sheath [30]. It is known that developmental hypothyroidism results in continued reduction of oligodendrocytes in the CC region from PND 10 [2]. In vitro study has shown that Cld11-overexpression results in induction of oligodendrocyte proliferation [31]. This result indicates that the overexpression of Cld11 at PND 20 is a compensatory response to decrease numbers of oligodendrocytes. However, mRNA levels were inconsistently decreased, suggesting involvement of post-transcriptional events such as those regulating mRNA stability and protein turnover.

DCC is a transmembrane receptor for netrin-1 via the fourth fibronectin type III domain [32]. Netrin-1 is a secreted protein, which elicits both attractive and repulsive responses in axonal guidance, neuronal migration and oligodendroglial migration depending on the homomeric or heteromeric combination of receptor dimers including DCC and Unc5 [33–35]. Netrin-1 signaling via DCC mediates growth cone extension and myelin sheath formation [36,37]. Therefore, increased expression of DCC in the myelin sheath at PND 20 induced by developmental hypothyroidism in the present study suggests a compensatory increase in response to suppression of myelin sheath formation [2]. However,

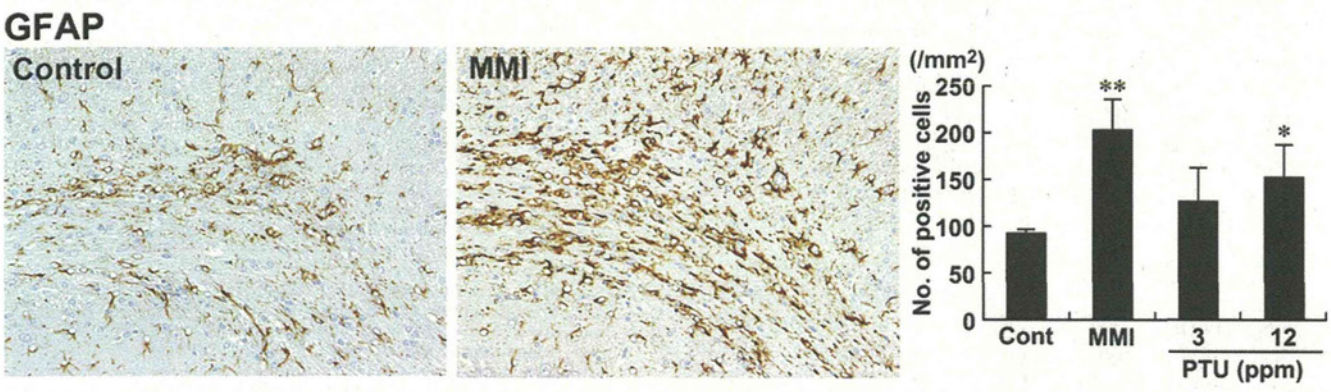

Fig. 6. Immunohistochemical distributions of GFAP-positive cells in the cingulum. Untreated control animal (left), MMI-treated animal (right). 200× magnification. Graph shows the mean number of positive cells within the cingulum at 200× magnification (untreated controls: $n = 6$; MMI and PTU groups: $n = 10$). $^{*}P < 0.05$, $^{**}P < 0.01$ vs. untreated controls.

DCC has an alternative function to drive cell death independent of both mitochondria-dependent and death receptor/caspase-8 pathways [38,39]. Moreover, DCC induces cell death in the absence of netrin-1 [40]. Because we did not find an increase in netrin-1 transcript levels using microarray analysis, it is possible that increased ligand-free DCC may lead to glial cell apoptosis. Progressive decrease in the CC area and the number of oligodendrocytes in this area during maturation after developmental hypothyroidism suggests the involvement of apoptosis due to increased ligand-free DCC [2,16].

Ret is a receptor protein–tyrosine kinase of glial cell line-derived neurotrophic factor (GDNF), a member of the transforming growth factor-β family [41]. GDNF signals play a critical role in development of the entire nervous system, kidney morphogenesis and spermatogenesis. While the functional relevance of Ret in oligodendrocytes has not been reported, this molecule is expressed in progenitor and immature oligodendrocytes in vitro and mediates cell proliferation induced by GDNF treatment [42]. Therefore, increased expression of Ret on PND 20 proceeding developmental hypothyroidism suggests a compensatory increase in response to decreased numbers of oligodendrocytes [2]. However, Ret induces cell death in the absence of its ligand similar to that of DCC [43]. Because we did not find an increase in GDNF transcript levels using microarray analysis, a progressive decrease in the size of the CC area and its oligodendrocyte density during maturation suggests involvement of apoptosis due to the increase of ligand-free Ret [2,16].

Vimentin is a member of the intermediate filament family of proteins. In the brain, this molecule is expressed in immature astrocytes during development [44–46]. Reactive astrocytes that are activated immature astrocytes during gliosis processes in response to injuries of CNS tissue also express vimentin [47,48]. Reactive astrocytes also express GFAP similar to that of mature astrocytes [47,48], suggesting that immature astrocytes can express both of vimentin and GFAP. On the other hand, developmental hypothyroidism leads to increase in vimentin expression in fetal rat brains [23]. Increase of GFAP-expression was also reported after developmental hypothyroidism in the CC region on PND 15 [49]. These results may suggest that developmental hypothyroidism increases the immature population of astrocytes. In the present study, vimentin-immunoreactive cells showed similar localization to those positive for GFAP. Therefore, a larger population of vimentin-positive cells in the cingulum induced by developmental hypothyroidism was considered to consist of immature astrocytes resembling reactive astrocytes. Interestingly, we previously reported frequent induction of subcortical band heterotopia in the CC, manifested by the appearance of aberrant cortical tissue in this anatomical area, in hypothyroid animals identical to the present study [16]. Anatomical location of this heterotopic tissue was close to the cingulum accumulating immature astrocytes, suggesting an etiological relation between the two. Alternatively, the increased immature astrocytes may simply be the reactive change in response to reduced oligodendrocytes due to developmental hypothyroidism [2,16,49]. However, developmental hypothyroidism may affect differentiation of neuronal progenitor cells, thereby inhibiting differentiation into oligodendrocytes, and instead, facilitating astrocytic differentiation during gliogenesis.

In conclusion, focusing on white matter development, we found aberrant expression of molecules associated with brain development after maternal exposure to anti-thyroid agents. Immunohistochemically, we found increased expression of Cld11, DCC, Ret and vimentin in white matter. Among them, vimentin and Ret were expressed in immature astrocytes and oligodendrocytes, respectively. Both positive cell populations were mainly distributed in the cingulum with the largest area of white matter. Because vimentin- and Ret-positive cells can be quantitatively evaluated, these molecules may be useful markers of glial cells, which respond to developmental exposure to thyroid hormone-disrupting chemicals.

Acknowledgments

We thank Tomomi Morikawa for her technical assistance in conducting the animal study. We also thank Ayako Kaneko for her technical assistance in preparing the histological specimens. This work was supported by Health and Labour Sciences Research Grants (Research on the Risk of Chemical Substances) from the Ministry of Health, Labour and Welfare of Japan. All authors disclose that there are no conflicts of interest that could inappropriately influence the outcome of the present study.

Appendix A. Supplementary data

Supplementary data associated with this article can be found, in the online version, at http://dx.doi.org/10.1016/j.reprotox.2012.03.005.

References

[1] Porterfield SP. Thyroidal dysfunction and environmental chemicals—potential impact on brain development. Environmental Health Perspectives 2000;108(Suppl. 3):433–8.
[2] Schoonover CM, Seibel MM, Jolson DM, Stack MJ, Rahman RJ, Jones SA, et al. Thyroid hormone regulates oligodendrocyte accumulation in developing rat brain white matter tracts. Endocrinology 2004;145:5013–20.
[3] Montero-Pedrazuela A, Venero C, Lavado-Autric R, Fernández-Lamo I, García-Verdugo JM, Bernal J, et al. Modulation of adult hippocampal neurogenesis by thyroid hormones: implications in depressive-like behavior. Molecular Psychiatry 2006;11:361–71.
[4] de Escobar GM, Obregón MJ, del Rey FE. Iodine deficiency and brain development in the first half of pregnancy. Public Health Nutrition 2007;10:1554–70.
[5] Comer CP, Norton S. Effects of perinatal methimazole exposure on a developmental test battery for neurobehavioral toxicity in rats. Toxicology and Applied Pharmacology 1982;63:133–41.
[6] Akaike M, Kato N, Ohno H, Kobayashi T. Hyperactivity and spatial maze learning impairment of adult rats with temporary neonatal hypothyroidism. Neurotoxicology and Teratology 1991;13:317–22.
[7] Guadaño Ferraz A, Escobar del Rey F, Morreale de Escobar G, Innocenti GM, Berbel P. The development of the anterior commissure in normal and hypothyroid rats. Brain Research Developmental Brain Research 1994;81:293–308.
[8] Lavado-Autric R, Ausó E, García-Velasco JV, Arufe Mdel C, Escobar del Rey F, Berbel P, et al. Early maternal hypothyroxinemia alters histogenesis and cerebral cortex cytoarchitecture of the progeny. Journal of Clinical Investigation 2003;111:954–7.
[9] Goodman JH, Gilbert ME. Modest thyroid hormone insufficiency during development induces a cellular malformation in the corpus callosum: a model of cortical dysplasia. Endocrinology 2007;148:2593–7.
[10] Shibutani M, Uneyama C, Miyazaki K, Toyoda K, Hirose M. Methacarn fixation: a novel tool for analysis of gene expressions in paraffin-embedded tissue specimens. Laboratory Investigation 2000;80:199–208.
[11] Uneyama C, Shibutani M, Masutomi N, Takagi H, Hirose M. Methacarn fixation for genomic DNA analysis in microdissected, paraffin-embedded tissue specimens. Journal of Histochemistry and Cytochemistry 2002;50:1237–45.
[12] Takagi H, Shibutani M, Kato N, Fujita H, Lee KY, Takigami S, et al. Microdissected region-specific gene expression analysis with methacarn-fixed, paraffin-embedded tissues by real-time RT-PCR. Journal of Histochemistry and Cytochemistry 2004;52:903–13.
[13] Shibutani M, Lee KY, Igarashi K, Woo GH, Inoue K, Nishimura T, et al. Hypothalamus region-specific global gene expression profiling in early stages of central endocrine disruption in rat neonates injected with estradiol benzoate or flutamide. Developmental Neurobiology 2007;67:253–69.
[14] Woo GH, Takahashi M, Inoue K, Fujimoto H, Igarashi K, Kanno J, et al. Cellular distributions of molecules with altered expression specific to thyroid proliferative lesions developing in a rat thyroid carcinogenesis model. Cancer Science 2009;100:617–25.
[15] Saegusa Y, Woo GH, Fujimoto H, Inoue K, Takahashi M, Hirose M, et al. Gene expression profiling and cellular distribution of molecules with altered expression in the hippocampal CA1 region after developmental exposure to anti-thyroid agents in rats. Journal of Veterinary Medical Science 2010;72:187–95.
[16] Shibutani M, Woo GH, Fujimoto H, Saegusa Y, Takahashi M, Inoue K, et al. Assessment of developmental effects of hypothyroidism in rats from in utero and lactation exposure to anti-thyroid agents. Reproductive Toxicology 2009;28:297–307.

[17] Masutomi N, Shibutani M, Takagi H, Uneyama C, Takahashi N, Hirose M. Impact of dietary exposure to methoxychlor, genistein, or diisononyl phthalate during the perinatal period on the development of the rat endocrine/reproductive systems in later life. Toxicology 2003;192:149–70.
[18] Nakamura R, Teshima R, Hachisuka A, Sato Y, Takagi K, Nakamura R, et al. Effects of developmental hypothyroidism induced by maternal administration of methimazole or propylthiouracil on the immune system of rats. International Immunopharmacology 2007;7:1630–8.
[19] Lee KY, Shibutani M, Inoue K, Kuroiwa K, U M, Woo GH, et al. Methacarn fixation—effects of tissue processing and storage conditions on detection of mRNAs and proteins in paraffin-embedded tissues. Analytical Biochemistry 2006;351:36–43.
[20] Ibarrola N, Rodríguez-Peña A. Hypothyroidism coordinately and transiently affects myelin protein gene expression in most rat brain regions during postnatal development. Brain Research 1997;752:285–93.
[21] Barradas PC, Vieira RS, De Freitas MS. Selective effect of hypothyroidism on expression of myelin markers during development. Journal of Neuroscience Research 2001;66:254–61.
[22] Farwell AP, Dubord-Tomasetti SA. Thyroid hormone regulates the expression of laminin in the developing rat cerebellum. Endocrinology 1999;140:4221–7.
[23] Evans IM, Pickard MR, Sinha AK, Leonard AJ, Sampson DC, Ekins RP. Influence of maternal hyperthyroidism in the rat on the expression of neuronal and astrocytic cytoskeletal proteins in fetal brain. Journal of Endocrinology 2002;175:597–604.
[24] Dasgupta A, Das S, Sarkar PK. Thyroid hormone promotes glutathione synthesis in astrocytes by up regulation of glutamate cysteine ligase through differential stimulation of its catalytic and modulator subunit mRNAs. Free Radical Biology and Medicine 2007;42:617–26.
[25] Royland JE, Parker JS, Gilbert ME. A genomic analysis of subclinical hypothyroidism in hippocampus and neocortex of the developing rat brain. Journal of Neuroendocrinology 2008;20:1319–38.
[26] Kobayashi K, Akune H, Sumida K, Saito K, Yoshioka T, Tsuji R. Perinatal exposure to PTU decreases expression of Arc, Homer 1, Egr 1 and Kcna 1 in the rat cerebral cortex and hippocampus. Brain Research 2009;1264:24–32.
[27] Bronstein JM, Popper P, Micevych PE, Farber DB. Isolation and characterization of a novel oligodendrocyte-specific protein. Neurology 1996;47:772–8.
[28] Bronstein JM, Micevych PE, Chen K. Oligodendrocyte-specific protein (OSP) is a major component of CNS myelin. Journal of Neuroscience Research 1997;50:713–20.
[29] Morita K, Sasaki H, Fujimoto K, Furuse M, Tsukita S. Claudin-11/OSP-based tight junctions of myelin sheaths in brain and Sertoli cells in testis. Journal of Cell Biology 1999;145:579–88.
[30] Gow A, Southwood CM, Li JS, Pariali M, Riordan GP, Brodie SE, et al. CNS myelin and sertoli cell tight junction strands are absent in Osp/claudin-11 null mice. Cell 1999;99:649–59.
[31] Tiwari-Woodruff SK, Buznikov AG, Vu TQ, Micevych PE, Chen K, Kornblum HI, et al. OSP/claudin-11 forms a complex with a novel member of the tetraspanin super family and beta1 integrin and regulates proliferation and migration of oligodendrocytes. Journal of Cell Biology 2001;153:295–305.
[32] Kruger RP, Lee J, Li W, Guan KL. Mapping netrin receptor binding reveals domains of Unc5 regulating its tyrosine phosphorylation. Journal of Neuroscience 2004;24:10826–34.
[33] Serafini T, Colamarino SA, Leonardo ED, Wang H, Beddington R, Skarnes WC, et al. Netrin-1 is required for commissural axon guidance in the developing vertebrate nervous system. Cell 1996;87:1001–14.
[34] Alcántara S, Ruiz M, De Castro F, Soriano E, Sotelo C. Netrin 1 acts as an attractive or as a repulsive cue for distinct migrating neurons during the development of the cerebellar system. Development 2000;127:1359–72.
[35] Spassky N, de Castro F, Le Bras B, Heydon K, Quéraud-LeSaux F, Bloch-Gallego E, et al. Directional guidance of oligodendroglial migration by class 3 semaphorins and netrin-1. Journal of Neuroscience 2002;22:5992–6004.
[36] Fazeli A, Dickinson SL, Hermiston ML, Tighe RV, Steen RG, Small CG, et al. Phenotype of mice lacking functional Deleted in colorectal cancer (Dcc) gene. Nature 1997;386:796–804.
[37] Rajasekharan S, Baker KA, Horn KE, Jarjour AA, Antel JP, Kennedy TE. Netrin 1 and Dcc regulate oligodendrocyte process branching and membrane extension via Fyn and RhoA. Development 2009;136:415–26.
[38] Forcet C, Ye X, Granger L, Corset V, Shin H, Bredesen DE, et al. The dependence receptor DCC (deleted in colorectal cancer) defines an alternative mechanism for caspase activation. Proceedings of the National Academy of Sciences of the United States of America 2001;98:3416–21.
[39] Furne C, Corset V, Hérincs Z, Cahuzac N, Hueber AO, Mehlen P. The dependence receptor DCC requires lipid raft localization for cell death signaling. Proceedings of the National Academy of Sciences of the United States of America 2006;103:4128–33.
[40] Mehlen P, Rabizadeh S, Snipas SJ, Assa-Munt N, Salvesen GS, Bredesen DE. The DCC gene product induces apoptosis by a mechanism requiring receptor proteolysis. Nature 1998;395:801–4.
[41] Sariola H, Saarma M. Novel functions and signalling pathways for GDNF. Journal of Cell Science 2003;116:3855–62.
[42] Strelau J, Unsicker K. GDNF family members and their receptors: expression and functions in two oligodendroglial cell lines representing distinct stages of oligodendroglial development. Glia 1999;26:291–301.
[43] Bordeaux MC, Forcet C, Granger L, Corset V, Bidaud C, Billaud M, et al. The RET proto-oncogene induces apoptosis: a novel mechanism for Hirschsprung disease. EMBO Journal 2000;19:4056–63.
[44] Pixley SK, de Vellis J. Transition between immature radial glia and mature astrocytes studied with a monoclonal antibody to vimentin. Brain Research 1984;317:201–9.
[45] Ciesielski-Treska J, Goetschy JF, Ulrich G, Aunis D. Acquisition of vimentin in astrocytes cultured from postnatal rat brain. Journal of Neurocytology 1988;17:79–86.
[46] Alonso G. Proliferation of progenitor cells in the adult rat brain correlates with the presence of vimentin-expressing astrocytes. Glia 2001;34:253–66.
[47] Pekny M, Wilhelmsson U, Bogestål YR, Pekna M. The role of astrocytes and complement system in neural plasticity. International Review of Neurobiology 2007;82:95–111.
[48] Eddleston M, Mucke L. Molecular profile of reactive astrocytes—implications for their role in neurologic disease. Neuroscience 1993;54:15–36.
[49] Sharlin DS, Bansal R, Zoeller RT. Polychlorinated biphenyls exert selective effects on cellular composition of white matter in a manner inconsistent with thyroid hormone insufficiency. Endocrinology 2006;147:846–58.

FULL PAPER *Surgery*

Pathological Classification of Canine Mammary Tumor Based on Quantifying mRNA Levels of Hormonal Receptors, SATB1, and Snail in Tissue and Fine Needle Biopsy Samples

Takahiro KOMATSU[1)], Hidetomo IWANO[2)], Masashi EBISAWA[2)], Ai WATABE[1)], Yoshifumi ENDO[1)], Kazuko HIRAYAMA[3)], Hiroyuki TANIYAMA[3)] and Tsuyoshi KADOSAWA[1)]*

[1)]*Veterinary Clinical Oncology, Department of Small Animal Clinical Sciences, School of Veterinary Medicine, Rakuno Gakuen University, Ebetsu, Hokkaido 069–8501, Japan*
[2)]*Department of Veterinary Biochemistry, School of Veterinary Medicine, Rakuno Gakuen University, Ebetsu, Hokkaido 069–8501, Japan*
[3)]*Department of Veterinary Pathology, School of Veterinary Medicine, Rakuno Gakuen University, Ebetsu, Hokkaido 069–8501, Japan*

(Received 28 September 2011/Accepted 23 December 2011/Published online in J-STAGE 10 January 2012)

ABSTRACT. Cytological diagnosis is not generally conclusive enough to identify histopathological malignancy in canine mammary tumors (CMTs). To establish cytological examination using fine needle biopsy (FNB) samples, gene expressions of hormonal receptors, human epidermal growth factor receptor 2 (HER2), and transcription regulators (Special AT-rich binding protein 1: SATB1 and Snail) were investigated in both tissue and FNB samples of CMTs. In tissue samples of malignant CMTs, especially invasive ones, low expressions of hormonal receptors and high expressions of SATB1 and Snail were detected. On discriminant analysis of tissue samples, 73.2% of CMTs were correctly classified according to histopathological examinations. In FNB samples of malignant CMTs, low expressions of hormonal receptors were detected. On discriminant analysis of FNB samples, 74.2% of CMTs were correctly classified according to histopathological examination. In conclusion, FNB gene expressions had a utility for diagnosis of CMTs malignancy in some degree. By researching more sensitive genes for malignant CMTs, the gene examination of FNB samples from CMTs will become a useful diagnostic tool that can be performed easily without anesthesia and could predict tumor malignancy and invasion prior to surgical removal.

KEY WORDS: canine, Fine Needle Biopsy, gene expression, mammary tumors.

doi: 10.1292/jvms.11-0440; *J. Vet. Med. Sci.* 74(6): 719–726, 2012

Canine mammary tumors (CMTs) are the most frequent neoplasms in female dogs. Based on the histopathological diagnosis, approximately half of CMTs is classified as malignant, and evaluation of tumor malignancy is clinically essential to determine the type of surgery [9, 17]. Histopathological diagnosis is the standard tool for determining tumor malignancy. However, most patients undergo surgical mammary gland removal without biopsy because general or local anesthesia is necessary to obtain tissue samples. On the other hand, fine needle biopsy (FNB) can be performed easily without anesthesia and is widely used to diagnose many types of tumors. However, cytological evaluation of CMTs is generally thought to be not conclusive enough to discriminate correctly between benign and malignant tumors [2]. Therefore, new cytological diagnostic tools that can be used for FNB samples are needed.

Recently, many proteins or gene expressions have been investigated for detecting tumor malignancy of CMTs. Lack of estrogen receptors (ER) and progesterone receptors (PR), which normal mammary glands should express, are well-known biomarkers associated with histologic tumor malignancy, lymph node involvement, and distant metastasis [11, 14, 26]. Moreover, in a study of ER and PR expression of 113 CMTs, lower PR expression was significantly associated with shorter survival times after surgical removal [11]. In recent years, human epidermal growth factor receptor 2 (HER2, c-erb-2) has been reported to have an important role in tumor aggressiveness. Its overexpression has been detected in 24–30% of human breast cancers [3, 30, 32]. Anti-HER2 antibody is widely used for HER2-overexpressing breast cancers as an antibody drug therapy. In the recent studies of HER2 expression of CMTs, overexpression of this protein was detected in 17.6–35.4% of malignant mammary tumors, and no or faint expression was seen in most benign mammary tumors [16, 20, 22, 25]. However, survival times and survival rates were better in dogs with HER2-overexpressing malignant mammary tumors than in dogs with tumors normally expressing HER2 [20].

These biomarkers, which are expected to be useful tools not only to classify CMTs as benign or malignant tumors but also to detect highly malignant, invasive tumors, were mainly evaluated using immunohistochemical (IHC) staining techniques. To identify gene biomarkers in CMTs, quantification of the mRNA levels of many genes, includ-

*CORRESPONDENCE TO: KADOSAWA, T., Veterinary Clinical Oncology, Department of Small Animal Clinical Sciences, School of Veterinary Medicine, Rakuno Gakuen University, Ebetsu, Hokkaido 069–8501, Japan.
e-mail: kado@rakuno.ac.jp

ing hormonal receptors and *HER2*, have been reported [21, 23, 31, 34]. In these studies, mRNA was extracted from mammary tumor tissue samples, but few reports assessed the gene expressions of biomarkers in FNB samples.

Special AT-rich binding protein 1 (SATB1) is a matrix attachment region (MAR)-binding protein and has emerged as a key factor for gene transcription. By regulating many gene expressions through remodeling chromatin architecture, SATB1 is thought to play an essential role in T cell differentiation and activation [4, 24]. Furthermore, this nuclear protein has a cage-like distribution and tethers chromatin loops to a distinct region as a genome organizer [10]. Recently, SATB1 expression has been investigated in some tumors, including human breast cancer [12, 18, 35]. Han *et al.* reported that high SATB1 expression level was correlated to a high tumor malignancy and poor prognosis in human breast cancer [18]. By reprogramming gene expression, SATB1 has been thought to make tumor cells more aggressive. Snail, which is the zinc finger transcription factor and one of the genes regulated by SATB1, has been described as a mediator of epithelial-mesenchymal transitions (EMTs) [6, 18]. EMTs are characterized by loss of cell adhesion molecules and gain of mesenchymal markers [33]. In human breast cancer, Snail was reported as an important key mediator of tumor cell invasion and metastasis by induction of EMT [7, 29]. However, the roles of SATB1 and Snail in CMTs have not been clear.

The aim of this study was to assess the utility of biomarkers for cytological examination to predict tumor malignancy and invasiveness by comparison of mRNA levels of *ER*, *PR*, *HER2*, *SATB1* and *Snail* between benign and malignant CMTs and between non-invasive and invasive CMTs, and to establish a new cytological gene examination using FNB samples.

MATERIALS AND METHODS

Patients: Fifty-five dogs studied included 14 Miniature Dachshunds, 6 Shih-Tzus, 4 Beagles, 3 each of Malteses, Papillons, and Shetland Sheepdogs, 2 each of American Cocker Spaniels, Miniature Schnauzers, Welsh Corgi Pembrakes, West Highland White Terriers, and Cavalier King Charles Spaniels, 1 each of Great Pyrenees, Poodle, Chihuahua, Japanese Spitz, and Miniature Bull Terrier, and 7 mixed breeds. These dogs had not had any malignant tumors before excisional biopsy except for the malignant mammary tumors. In 15 dogs, ovariohysterectomy (OHE) had been performed prior to the removal of CMTs. One dog with a mammary tumor was male. The dogs' mean age at the time of tumor removal was 10.0 years (range, 4 to 16 years).

Samples: Fifty-six tissue samples were obtained by excisional surgery from 55 dogs with mammary tumors. The tissue samples under 0.03 grams were obtained from the marginal tumor tissues of the specimens. The mean size of the CMTs was 2.9 cm (range, 0.5 to 11 cm). FNB samples were obtained by inserting 22-G needles into the tumors through the skin in 31 CMTs prior to tissue sample collection. After these sampling, mammary tumors were examined histopathologically by a veterinary pathologist and classified according to the WHO classification [28]. Based on the histopathological examination, the CMTs were categorized into benign or malignant, and non-invasive or invasive. Invasive tumor was defined as tumor with infiltrative growth into the surrounding normal tissues or lymph and blood vessels. All tissue or cytological samples were immersed with RNA*later* (Applied Biosystems, Foster City, CA, U.S.A.) overnight at 4°C or 30 min on ice, followed by removal of the RNA*later* and storage at −80°C.

RNA isolation and reverse transcription polymerase chain reaction (RT-PCR): Total RNA was isolated from mammary tumors using an RNeasy Mini kit (Qiagen, Hilden, Germany). DNAse digestion was performed using an RNase-Free DNase kit (Qiagen). cDNA was synthesized from 1 μg of tRNA with ReverTra Ace reverse transcriptase (Toyobo, Osaka, Japan) and oligo dT primers (Toyobo) according to the manufacturer's instructions.

Quantitative RT-PCR (qRT-PCR) analysis: cDNA that had been diluted for the amplification of the target genes (*ER*, *PR*, *HER2*, *SATB1*, and *Snail*) was used for qRT-PCR analysis. A standard curve for each gene was produced using 100- and 10-fold serial dilutions of the genes as a template (10^8, 10^6, 10^4, and 10^3 copies). The reaction was performed using a Quantitect SYBR Green PCR kit (Qiagen) and an iQ5/MyiQ Single-Color (Bio-Rad Laboratories, Hercules, CA, U.S.A.) following the manufacturer's instructions, run as triplicates of each sample. The copy number of each gene expressed in CMTs was calculated from a standard curve and normalized to that of *ribosomal protein 19 (RP19)*. Each primer sequence is shown in Table 1.

Statistical analysis: The Mann-Whitney U test was used to analyze the differences in the mRNA expression levels of target genes between benign and malignant CMTs, and between non-invasive and invasive CMTs, with $P<0.05$ considered significant. The genes that had significantly different expressions among these categories were selected for discriminant analysis. Each tumor sample was classified into these categories by discriminant analysis. The relationship between tissue and FNB samples in gene expression was analyzed by Spearman's rank correlation coefficient. Data analyses were carried out with Excel Toukei 2010 (SSRI, Tokyo, Japan).

RESULTS

Histologic study: The 56 tissue samples consisted of 28 benign CMTs (2 simple adenomas, 18 complex adenomas, 8 mixed tumors) and 28 malignant CMTs (12 simple carcinomas, 13 complex carcinomas, 1 adenocarcinoma, 1 carcinosarcoma, 1 osteosarcoma); of the malignant CMTs, 16 showed tumor invasiveness to the surrounding normal tissues or lymph and blood vessels.

Gene expressions and discriminant analysis of tissue samples: The expression level of *ER* appeared significantly higher in benign (median, 0.01; average, 0.03) CMTs than in malignant (median, 0.002; average, 0.006) CMTs. The difference in *ER* expression between non-invasive (median,

Table 1. Primer nucleotide sequences

Gene	Nucleotide sequence (5' to 3')	Size (bp)	Accession No.
ERα	F: CCTTCAGTGAAGCTTCGATG	130	XM_533454
	R: AGAAGGTGGACCTGATCATG		
PR	F: CAGGAAGAGTTCCTGTGTAT	255	NM_001003074
	R: CCGGGACTGGATAAATGTAT		
HER2	F: CAGCCCTGGTCACCTACAA	120	NM_001003217
	R: CCACATCCGTAGACAGGTAG		
SATB1	F: GATTCAGCAGGAAATGAAGCG	211	XM_542770
	R: GCTCTCCTGTTCATAAATGGC		
Snail	F: GACTCCCAGACTCGCAAGG	308	XM_543048
	R: GACATGCGGGAGAAGGTTCG		
RPI9	F: CCTTCCTCAAAAAGTCTGGG	95	XM_538673
	R: GTTCTCATCGTAGGGACGAAG		

F, forward; R, reverse.

0.01; average, 0.02) and invasive (median, 0.001; average, 0.004) CMTs was also significant (Fig. 1A). The tissue samples of spayed dogs expressed *ER* (median, 0.004; average, 0.009) less than those of intact dogs (median, 0.009; average, 0.020). The expression levels of *PR* were also significantly higher in benign (median, 0.05; average, 0.07) CMTs and in non-invasive (median, 0.03; average, 0.06) CMTs than in malignant (median, 0.006; average, 0.02) CMTs and invasive (median, 0.008; average, 0.02) CMTs (Fig. 1B). The tissue samples of spayed dogs expressed *PR* (median, 0.009; average, 0.02) less than those of intact dogs (median, 0.03; average, 0.06). The expression levels of *HER2* were similar in benign (median, 0.02; average, 0.04) and malignant (median, 0.02; average, 0.03) CMTs, and non-invasive (median, 0.02; average, 0.04) and invasive (median, 0.01; average, 0.03) CMTs (Fig. 1C). The expression levels of *SATB1* were similar in benign (median, 0.1; average, 0.15) and malignant (median, 0.1; average, 0.2) CMTs, but expression levels were significantly higher in invasive (median, 0.14; average, 0.33) CMTs than in non-invasive (median, 0.09; average, 0.13) CMTs (Fig. 1D). In particular, *SATB1* expression levels were high in samples from patients that had a relapse of CMTs or died within six months after tumor excision (data not shown). *Snail* was similarly expressed in benign (median, 0.05; average, 0.05) and malignant (median, 0.06; average, 0.16) CMTs, but there was a significant difference in *Snail* expression between non-invasive (median, 0.04; average, 0.07) and invasive (median, 0.07; average, 0.2) CMTs (Fig. 1E). To predict the histological malignancy of each tumor based on gene expression, *ER* and *PR*, which showed significant differences between benign and malignant CMTs, were used for the discriminant analysis. The total accuracy of classification was 73.2% (Table 2A). Four genes (*ER*, *PR*, *SATB1*, and *Snail*) that had significant differences between non-invasive and invasive CMTs were used for the discriminant analysis to predict tumor invasiveness. The total accuracy of classification was 80.0% (Table 2B).

Gene expressions and discriminant analysis of FNB samples: Quantification of gene expressions was performed in 31 FNB samples from the CMTs, including 21 benign and 10 malignant CMTs. Seven FNB samples were from invasive CMTs. *HER2* was excluded from the target genes for FNB analysis because of the tissue sample results. Significant differences in *ER* expressions that were observed in tissue samples were well preserved in FNB samples. High expressions of *ER* in benign (median, 0.06; average, 0.08) and non-invasive (median, 0.05; average, 0.08) CMTs and low expressions of *ER* in malignant (median, 0.002; average, 0.008) and invasive (median, 0.002; average, 0.005) CMTs were identified in FNB samples (Fig. 2A). *PR* expression levels of FNB samples were significantly higher in benign (median, 0.07; average, 0.15) CMTs than in malignant (median, 0.004; average, 0.008) CMTs (Fig. 2B). Moreover, a difference in *PR* expression was also detected between non-invasive (median, 0.06; average, 0.13) and invasive (median, 0.004; average, 0.007) CMTs. However, a tendency for higher expressions of *SATB1* and *Snail* in invasive tissue samples was not detected in FNB samples (Fig. 2C and 2D). On discriminant analysis of FNB samples, *ER* and *PR* were used for classification, along with both tumor malignancy and invasiveness. Using the two genes, 61.9% of benign and 100% of malignant CMTs, as well as 62.5% of non-invasive and 100% of invasive CMTs, were correctly classified (total accuracy was 74.2 and 71.0%, respectively) (Table 3A and 3B). In addition, expression levels of *ER*, *PR*, *SATB1*, and *Snail* in FNB samples were compared with each of their expression levels in the tissue samples. *ER* and *PR* had positive correlations (r_s=0.74, P<0.01 and r_s=0.83, P<0.01, respectively), but *SATB1* and *Snail* had no correlation (r_s=−0.08, P>0.05 and r_s=0.18, P>0.05, respectively).

DISCUSSION

Recently, the expressions of many genes and proteins in tissues from CMTs have been investigated, and differences in expressions between benign and malignant CMTs have been reported. In the present study, to establish a cytological gene examination that could be easily performed prior to definitive surgical therapy, tissues and FNB samples from CMTs were used for detecting mRNA levels of *ER*, *PR*, *HER2*, *SATB1*, and *Snail*.

It is widely known that protein expressions of ER and

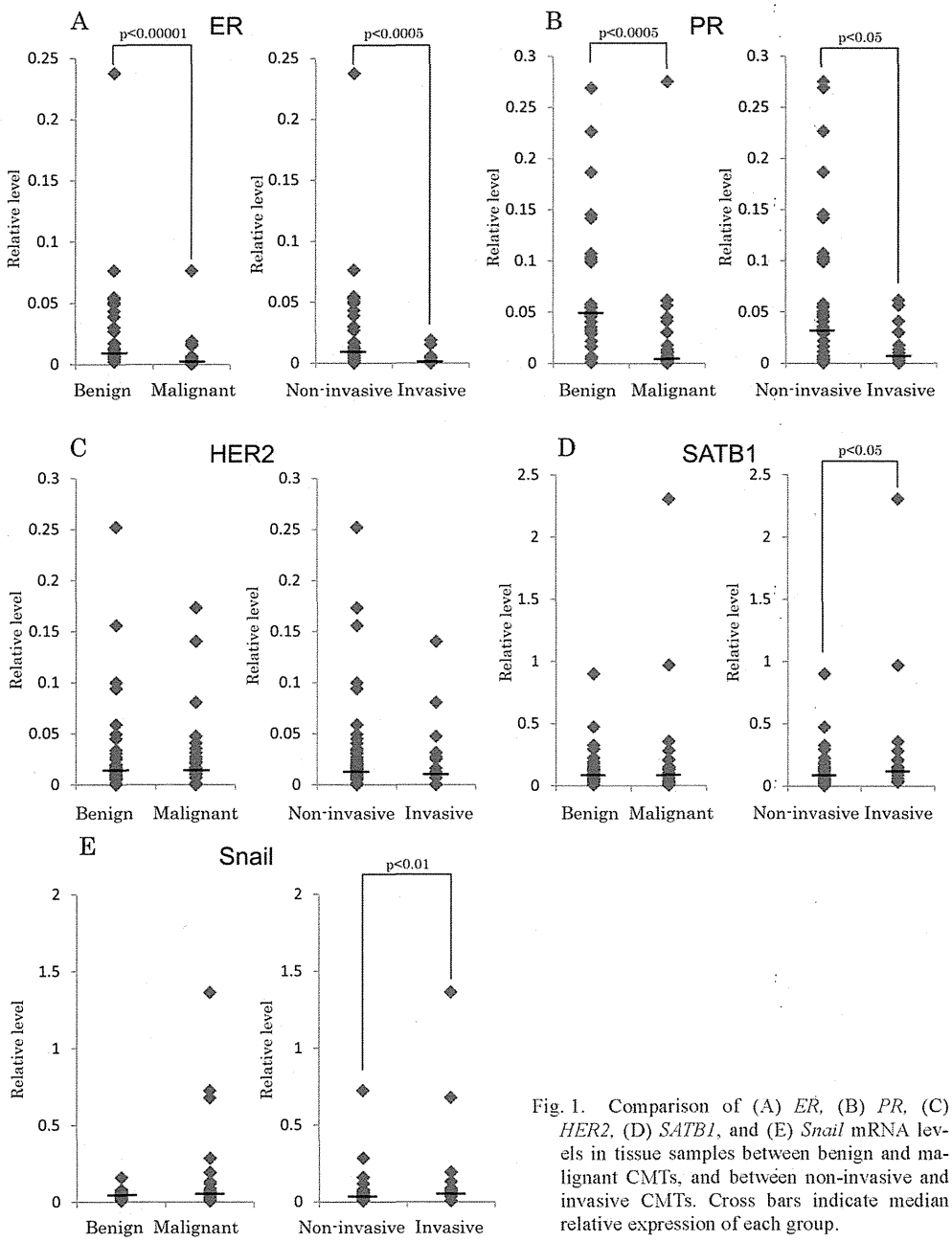

Fig. 1. Comparison of (A) *ER*, (B) *PR*, (C) *HER2*, (D) *SATB1*, and (E) *Snail* mRNA levels in tissue samples between benign and malignant CMTs, and between non-invasive and invasive CMTs. Cross bars indicate median relative expression of each group.

PR decrease in malignant CMTs. Similarly, in the present study, gene expressions of *ER* and *PR* in the tissue samples were lower in malignant CMTs than in benign CMTs, and the tissue samples from spayed dogs expressed these genes less than the samples from intact dogs. These data suggested that gene expression levels of *ER* and *PR* have a relative correlation with their protein expression levels and would be useful diagnostic tools to detect the malignancy of CMTs. In addition, *ER* and *PR* showed lower expression levels in invasive CMTs than in non-invasive CMTs. Hashimoto *et al.* also reported that protein concentrations of ER and PR decreased in proportion to progression in the clinical stage of CMTs [19]. These results indicated that *ER* and *PR* could predict CMT invasiveness. On the other hand, higher gene expressions of *ER* and *PR* in benign CMTs were detected in FNB samples, as well as in tissue samples. Thus, *ER* and *PR* might be suitable biomarkers for gene examination of CMTs using FNB samples. This would provide valuable information to help determine whether ovariohysterectomy should be done along with removal of CMTs.

Table 2. Discriminant analysis with *ER*, *PR*, *SATB1* and *Snail* expressions

A. Classification of tissue samples by the histological malignancy

Histopathological tumor type	Result of classification by discriminant analysis		Accuracy
	Benign	Malignant	
Benign (n=28)	15	13	53.60%
Malignant (n=28)	2	26	92.90%
		All samples	73.20%

B. Classification of tissue samples by the tumor invasiveness

Histopathological tumor type	Result of classification by discriminant analysis		Accuracy
	Non-invasive	Invasive	
Non-invasive (n=40)	38	2	95.00%
Invasive (n=16)	9	7	43.80%
		All samples	80.00%

Table 3. Discriminant analysis with ER and PR expressions

A. Classification of FNB samples by the histological malignancy

Histopathological tumor type	Result of classification by discriminant analysis		Accuracy
	Benign	Malignant	
Benign (n=21)	13	8	61.90%
Malignant (n=10)	0	10	100.00%
		All samples	74.20%

B. Classification of FNB samples by the tumor invasiveness

Histopathological tumor type	Result of classification by discriminant analysis		Accuracy
	Non-invasive	Invasive	
Non-invasive (n=24)	15	9	62.50%
Invasive (n=7)	0	7	100.00%
		All samples	71.00%

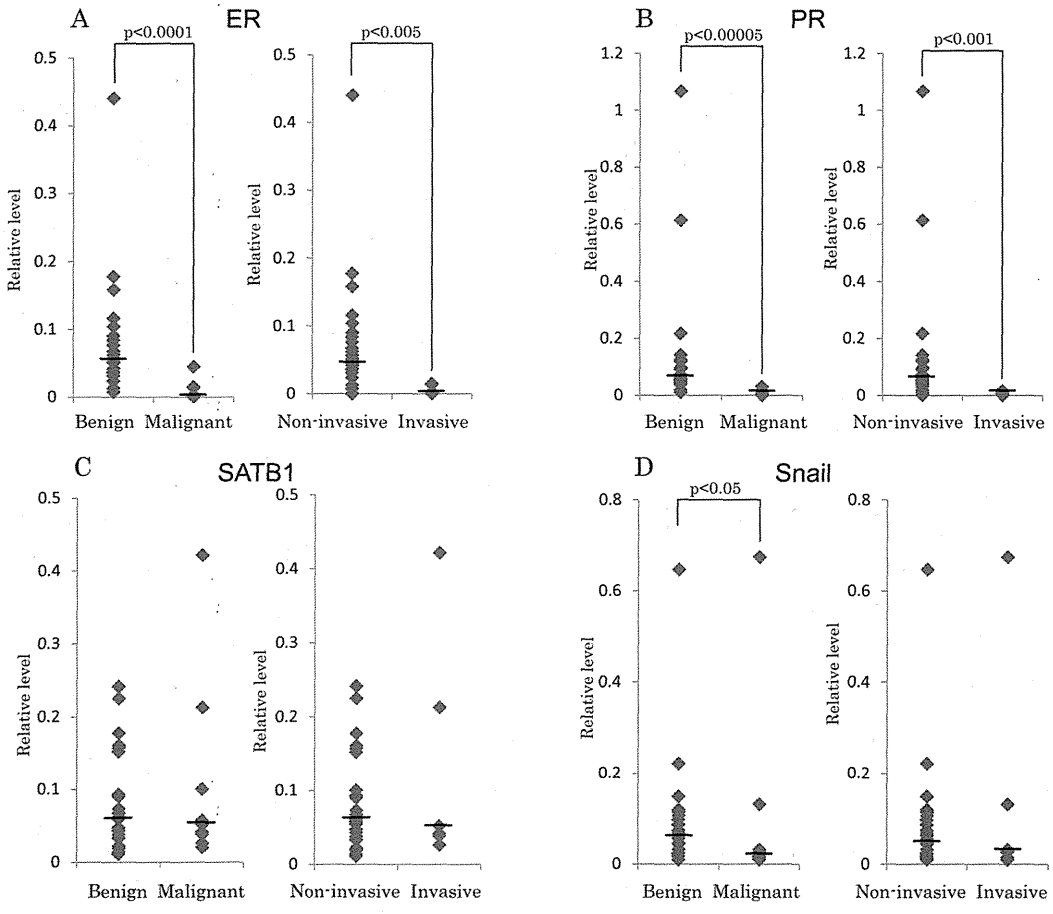

Fig. 2. Comparison of (A) *ER*, (B) *PR*, (C) *SATB1*, and (D) *Snail* mRNA levels in FNB samples between benign and malignant CMTs, and between non-invasive and invasive CMTs. Cross bars indicate median relative expression of each group.